Chapter 16

Deep Inelastic Scattering of (Anti)neutrinos from Nuclei

16.1 Introduction

We have discussed charged lepton and (anti)neutrino induced deep inelastic scattering (DIS) off free protons in Chapter 13. The interaction cross section and the structure functions of nucleons are modified when the scattering takes place from the nucleons bound inside a nucleus. The reactions are shown in Figure 16.1, where $l = e, \mu$. A is the target nucleus and X is the jet of hadrons. k, p and k', p' are the four momenta of the initial and the final state particles respectively. Historically, the first observations of modifications of the nuclear structure

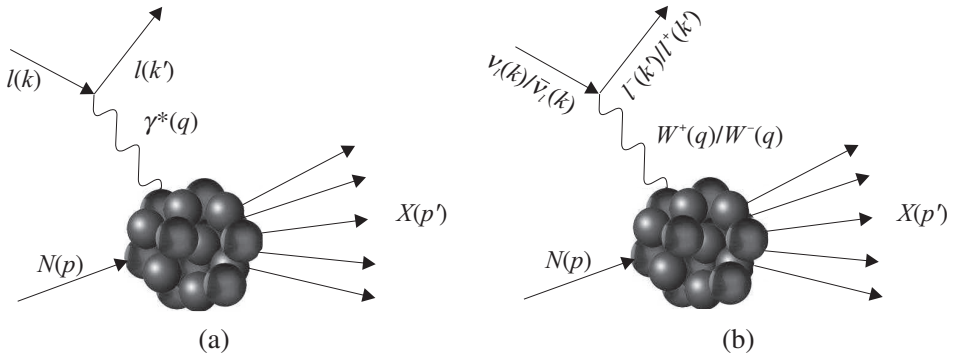

Figure 16.1 The deep inelastic charged lepton (a) and (anti)neutrino (b) scattering processes with bound nucleons for the electromagnetic and weak interactions, respectively.

functions were made by the European Muon Collaboration (EMC) at CERN in 1981–83. The EMC collaboration studied the ratio of structure function $F_2(x, Q^2)$ per nucleon for iron to deuterium targets, that is, $R(x, Q^2) = \frac{F_{2Fe}(x,Q^2)/A}{F_{2D}(x,Q^2)/2}$ in the energy region of 120-280 GeV and

https://doi.org/10.1017/9781108489065.017 Published online by Cambridge University Press

its deviation from unity. This effect is known as the EMC effect. Since then, the EMC effect has been confirmed and studied with improved precision in many DIS experiments using electrons, muons [783, 784, 785, 786, 787, 788], neutrinos, and antineutrinos [789, 790, 791, 792, 793, 794] from different nuclear targets as well as in the Drell–Yan processes using proton and pions [795, 796, 797]. Some of these results are presented in Figure 16.2. From the figure, it may be observed that the ratio is different from unity in almost the entire region of the Bjorken scaling variable $0 < x < 1$. From these experiments, some general features of the ratio $R(x, Q^2)$ may be inferred:

- The x dependence of $R(x, Q^2)$ has considerable structure, that is, it is different in different regions of x.
- The shape of the effect is almost independent of A.
- The functional form of $R(x, Q^2)$ is relatively independent in the region of high Q^2.

Generally, the nuclear medium effects manifested through the ratio $R(x, Q^2)$ are broadly divided into four regions of x in which the x dependence is attributed to different physical effects. These are:

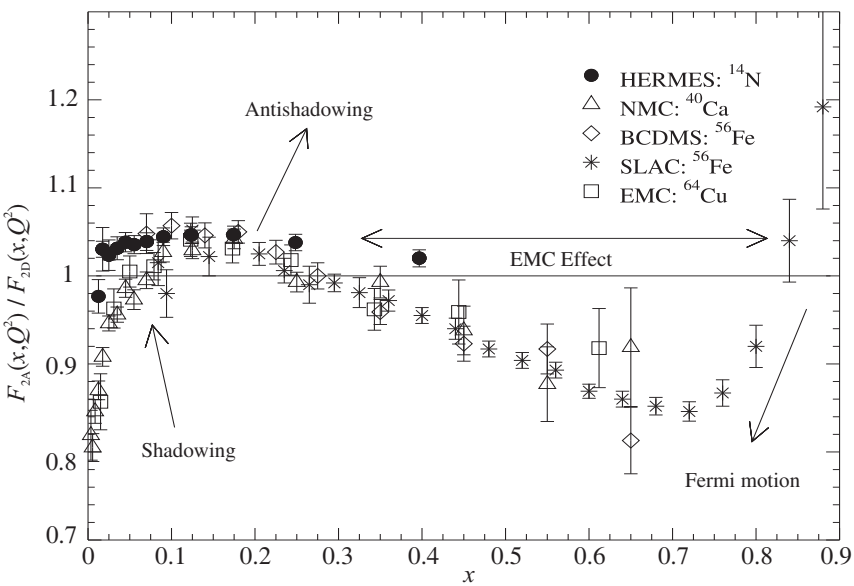

Figure 16.2 Ratio $R(x, Q^2) = \frac{F_{2A}(x,Q^2)}{F_{2D}(x,Q^2)}$; ($A$ = target nucleus) vs. x shows the nuclear medium effects in structure function. Experimental data are taken from the Refs. [783, 786, 787, 797, 784].

1. **Shadowing effect:** In the region of low $x(< 0.1)$, a suppression is found in the ratio $R(x, Q^2) = \frac{F_{2A}(x,Q^2)}{F_{2D}(x,Q^2)}$ which is known as the shadowing effect. This suppression becomes more pronounced with the increase in the mass number A.

https://doi.org/10.1017/9781108489065.017 Published online by Cambridge University Press

2. **Antishadowing effect:** This is the region of $0.1 \leq x \leq 0.2$, where there is an enhancement in the ratio of structure functions ($R(x, Q^2)$); the region has been found to have almost no nuclear mass dependence.
3. **EMC effect:** The ratio $R(x, Q^2)$ shows a dip in the region of $0.2 < x < 0.7$; this is known as the EMC effect, named after the first experimental observation by the EMC collaboration [798].
4. **Fermi motion:** The nucleons bound inside the nuclear target move with some Fermi momentum which increases with the increase in the mass number. This is a kinematic effect and is responsible for the abrupt rise in the ratio of structure functions in the region of higher $x \geq 0.7$.

The discovery of the EMC effect was unexpected and quite surprising in view of the very high energy and momentum transfers involved in the DIS process which are several orders of magnitude larger than the binding energy and Fermi momentum of nucleons inside the nucleus. The possibility that the role of quarks and gluons may be modified in the nuclear environment was anticipated and discussed earlier by the nuclear physics community but the evidence of large nuclear effects as seen in the EMC experiment was surprising.

In this chapter, we will focus on the experimental and theoretical studies of the DIS of (anti)neutrinos from nuclear targets and the effect of a nuclear medium on cross sections and structure functions.

16.2 DIS from Bound Nucleons

In the DIS using charged lepton or (anti)neutrino scattering from bound nucleons in the nucleus, the nuclear medium effects play a very important role. There are various types of nuclear effects which can be classified as follows:

(i) **Binding energy and Fermi motion effects**
The binding energy and the Fermi motion of the bound nucleons affect the kinematics as well as the dynamics of the DIS process induced by both the charged lepton and (anti)neutrinos from the nuclear targets. For example, the invariant mass W of the charged lepton (neutrino) and bound nucleon is given by

$$W^2 = (p+q)^2 \geq (M+m_\pi)^2 \tag{16.1}$$

to initiate the inelastic processes. Since

$$W^2 = p^2 + q^2 + 2p\cdot q = q^2 + (M-\varepsilon)^2 + 2q_0(M-\varepsilon) - \vec{p}\cdot\vec{q}, \tag{16.2}$$

where ε is the separation energy of the bound nucleon, the kinematics of the DIS process is modified due to the nucleon target being bound. Moreover, the bound nucleons can have any momentum $\vec{p}$ lying between $0 < |\vec{p}| < p_F$, where p_F is the Fermi momentum (Chapter 14). Therefore, an integration of the cross section and structure functions over

https://doi.org/10.1017/9781108489065.017 Published online by Cambridge University Press

all the momentum weighted by the nucleon spectral function describing the momentum distribution is required to be performed. There are many models for the nucleon spectral function discussed in literature [799, 800, 801, 802, 803, 804, 805].

(ii) **Off shell effect**

The bound nucleons, that is, protons and neutrons in a nucleus are not on-shell, in other words $p^2 \neq M^2$. Therefore, the structure functions will not only depend upon the variables ν and Q^2 (or x in the scaling region) but also on the off shell virtuality (χ) of the particle measured by $\chi = \frac{p^2 - M^2}{M^2}$. Moreover, being off shell, the nucleons do not satisfy the Dirac equation. Therefore, the electromagnetic (weak) structure functions will not be described in terms of only two (three) structure functions, but more than two (three) structure functions which vanish for $p^2 = M^2$. While the corrections to the existing structure functions $F_2^{\mathrm{EM}}(x, Q^2)$ and $F_2^{\mathrm{WI}}(x, Q^2)$ due to $\chi \neq 0$ have been calculated by doing an expansion in the powers of χ, the additional structure functions have not been studied much in literature. However, in case of many nuclei, the virtuality is quite small; therefore, the cross section can still be described by on-shell structure functions [799, 800].

(iii) **Mesonic effects**

Most low energy nuclear processes are very well described in impulse approximation (IA). However, there are certain processes even in the region of low and intermediate energies, where the interaction takes place from the mesons in flight between the two bound nucleons; these are called meson exchange current (MEC) effects [806, 807, 808]. In the case of DIS, the meson cloud of nucleons are taken into account in the evaluation of the nucleon structure functions. The charged lepton and (anti)neutrinos can also scatter from mesons like π and ρ in the nuclear volume. Since these mesons are also off-shell, their meson off-shell structure functions need to be calculated in order to estimate their contributions to the nuclear structure functions. The contribution from the meson structure functions are calculated in a model similar to the model used for nucleons utilizing free meson structure functions and convoluting them with the momentum distribution of mesons [809].

(iv) **Effect of short range correlations (SRC) and multiquark clusters**

In the conventional picture of nuclei, the nucleons move in the central or mean field leading to the various nuclear states which describe the static properties of nuclei and nuclear transitions induced by photons, leptons, and hadrons. This also leads to an average density of the nucleus. The DIS cross section and the EMC effect seem to depend upon the average density. However, in various nuclei, especially at low A, there is evidence of the local density being higher than the average density leading to clustering. The clustering of nucleons leading to the cluster model of nuclei is well known for nuclear phenomenon at low and intermediate energies. In the region of high energy and momentum transfers, where quarks and gluons are expected to play a significant role, multiquark clustering may also be present. For example, in the DIS of electron from nuclei, there is some evidence that there exists a 20–30% probability of 6-quark clustering.

https://doi.org/10.1017/9781108489065.017 Published online by Cambridge University Press

The α-cluster model description of ^{8}Be, ^{9}Be, ^{12}C, and $(\alpha - d)$ cluster model of ^{6}Li has been quite successful in describing nuclear phenomenon. This type of clustering can arise due to the short range correlations (SRC) between nucleons. Such SRC are well known leading to pairing even in intermediate and high A nuclei. Due to SRC and clustering, there would be considerable overlap of nucleons leading to quark exchange between the two nucleons. The $p - n$ correlations are known to be stronger than the $p - p$ and $n - n$ correlations, affecting the proton structure functions more than the neutron structure functions in nuclei.

Recent experiments of DIS for electrons at JLab from light nuclei like ^{4}He, ^{9}Be and ^{12}C, the observations show that the cross sections and EMC effect depend upon the local density, which is considerably higher than the average density of the nuclei.

(v) **Non-isoscalarity**
In defining the ratio $R(x, Q^2)$, the cross section per nucleon or the structure function per nucleon for nuclear targets used in the numerator corresponds to isoscalar nuclei which is obtained after applying corrections due to $N \neq Z$ in some nuclear targets like ^{56}Fe or ^{208}Pb. Similarly, in the denominator, $F_2^D = \frac{F_2^p + F_2^n}{2}$, where it is taken to be the average of structure functions for protons and neutrons. The structure function for the neutron is obtained from the DIS experiments performed on the deuterium target; deuterium corrections are then applied. In this case, the nuclear effects in the deuterium are calculated. While there are many calculations of nuclear effects in deuterium, there are no comprehensive theoretical studies of the non-isoscalarity corrections in the heavier nuclei. In the case of heavier nuclei, such corrections are calculated phenomenologically for the DIS of electrons; the same are applied in the case of neutrino scattering.

(vi) **Multiple scattering**
The DIS of charged leptons and (anti)neutrinos are understood in terms of the interaction of virtual photons and $W^{\pm}(Z^0)$ bosons with partons. In a nucleus, these virtual photons and $W^{\pm}(Z^0)$ bosons traverse the nuclear medium before scattering with the partons. During the passage, the particles may undergo hadronization, that is, fluctuate momentarily into hadrons or quark–antiquark pairs and gluons, which then undergo scattering with nuclear constituents through strong interactions leading to substantial modification in the cross sections in some kinematic regions. This is typical of a nuclear medium effect; there is considerable evidence of this type of scattering taking place in nuclei.

It is not possible to go into the details of all the nuclear medium effects described here. However, we will describe some of the effects which make dominant contribution to the structure function in the following sections, focusing on the DIS of (anti)neutrino from nuclear targets.

First, we shall discuss the phenomenological approaches which are used to extract the nuclear medium effects in the DIS of the charged lepton-, (anti)neutrino- nucleus scattering as well as the Drell–Yan processes in proton–nucleus and pion–nucleus scattering experiments.

https://doi.org/10.1017/9781108489065.017 Published online by Cambridge University Press

16.3 Extraction of Structure Functions from Cross Section Measurements

The DIS scattering cross sections for the charged lepton as well as the (anti)neutrino induced processes have been measured in various experiments [810, 811, 566, 562, 561]. The structure functions are extracted from these cross section measurements, after making a suitable choice of the kinematical variables and making some reasonable assumptions about the structure functions $F_i(x, Q^2)(i = 1, 2, 3, L)$. In the case of electromagnetic interaction, the cross sections are expressed in terms of the longitudinal and transverse structure functions (Chapter 13) which are respectively described by $F_{\rm LN}(x, Q^2)$ (Eq. (13.46)) and $F_{1N}(x, Q^2)$ (Eq. (13.45)). The separation of longitudinal and transverse cross sections is generally done by using the Rosenbluth technique [812]. This technique involves the measurements of cross sections at two (at least) or more values of photon polarization vector (ϵ) obtained at fixed (x, Q^2). A linear fit is performed as shown in Figure 16.3. In this way, one may extract $F_i(x, Q^2)(i = 1, 2, L)$

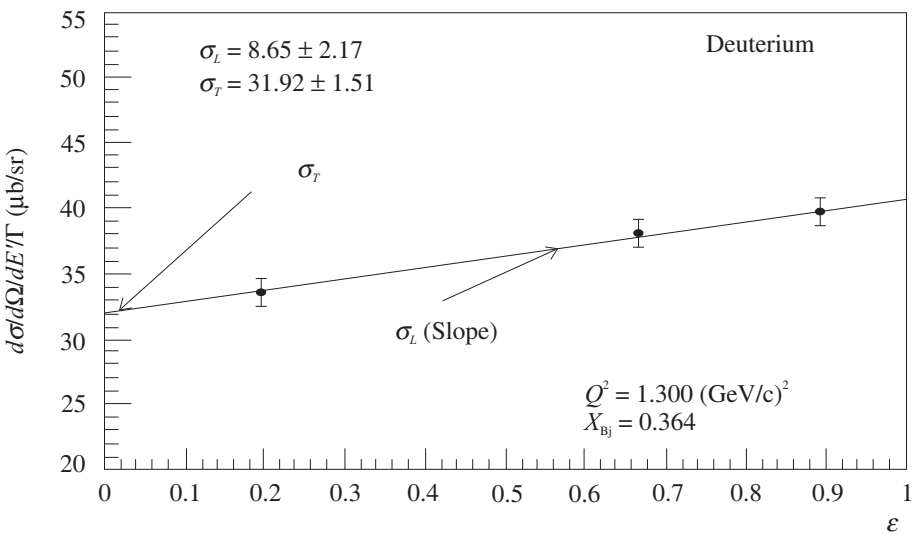

Figure 16.3 σ_L and σ_T separation using Rosenbluth technique [813].

(Eqs. (13.45) and (13.46)) and $R_L(x, Q^2)$ (Eq. (13.43)) using the cross section measurements on $\sigma_T(x, Q^2)$ and $\sigma_L(x, Q^2)$. A parameterization of $R_L(x, Q^2)$ has been given by Whitlow et al. [810] using the $e - p$ and $e - d$ scattering data from SLAC:

$$\begin{aligned} R_L(x, Q^2) &= \frac{0.0635}{\ln(Q^2/0.04)}\Theta(x, Q^2) + \frac{0.5747}{Q^2} - \frac{0.3534}{Q^4 + 0.09}, \\ \text{where} \quad \Theta(x, Q^2) &= 1 + 12\left(\frac{Q^2}{1 + Q^2}\right)\left(\frac{0.125^2}{x^2 + 0.125^2}\right). \end{aligned} \tag{16.3}$$

It is important to notice (Eq. (13.47)) that for the extraction of $F_2(x, Q^2)$, the precise measurement of $R_L(x, Q^2)$ is required which is planned to be determined in several nuclear targets in future experiments at the JLab.

https://doi.org/10.1017/9781108489065.017 Published online by Cambridge University Press

In the case of (anti)neutrino scattering, the early experiments from the nuclear targets in the high energy region were done at CERN; later experiments at FNAL, BNL, ITEP, JINR, etc. were performed by using the nucleon and nuclear targets in the lower energy region (see Table 16.1). For example, in the NuTeV [566], high statistics measurements of the differential

Table 16.1 Some of the experiments which studied (anti)neutrino induced DIS cross section and structure functions from nuclear targets.

Experiment	Laboratory	Target	Energy range (GeV)
CCFR-I			30–300
CCFR-II	FNAL	Fe	30–300
CCFR-III			30–360
CDHSW	CERN	Fe	20–212
CHARM	CERN	$CaCO_3$	10–160
CHARM-II	CERN	glass	5–100
BEBC	CERN	Ne (D_2)	15–160
NuTeV	FNAL	Fe	30–360
NOMAD	CERN	C, Fe	5–200
CHORUS	CERN	Emulsion, Pb	10–200

cross section were performed using neutrino and antineutrino beams on an iron target. The extraction of structure functions can be made by using the neutrino and antineutrino scattering cross sections

$$\begin{aligned}\frac{d^2\sigma_N^{\rm WI}}{dxdy} &= \frac{G_F^2\, s}{2\pi}\left[\left(1-y-\frac{Mxy}{2E_l}+\frac{y^2}{2}\frac{1+4M^2x^2/Q^2}{1+R_L}\right)F_{2N}^{\rm WI}(x,Q^2)\right.\\ &\left.\pm xy\left(1-\frac{y}{2}\right)F_{3N}^{\rm WI}(x,Q^2)\right]\ , \end{aligned} \tag{16.4}$$

which is obtained by using Eq. (13.66) and the modified Callan–Gross relation, Eq. (13.47). In Eq. (16.4), a positive sign corresponds to the neutrino and a negative sign to the antineutrino. Using Eq. (16.4), the expression for the sum of the neutrino and antineutrino induced DIS cross section may be written as:

$$\begin{aligned}\frac{d^2\sigma^{\nu}}{dx\,dy}+\frac{d^2\sigma^{\bar\nu}}{dx\,dy} &= \frac{G_F^2\, s}{2\pi}\left[2\left(1-y-\frac{Mxy}{2E_l}+\frac{y^2}{2}\frac{1+4M^2x^2/Q^2}{1+R_L}\right)F_{2N}^{\rm avg}\right.\\ &\left.+y(1-\frac{y}{2})\Delta xF_{3N}\right], \end{aligned} \tag{16.5}$$

where $F_{2N}^{\rm avg}(=\frac{1}{2}[F_{2N}^{\nu}+F_{2N}^{\bar\nu}])$ is the average of F_{2N}^{ν} and $F_{2N}^{\bar\nu}$ and $\Delta xF_{3N}=[xF_{3N}^{\nu}-xF_{3N}^{\bar\nu}]$. At the leading order, ΔxF_{3N} is given by [566]

$$\begin{aligned}\Delta xF_{3N} &= 2x(s+\bar s-c-\bar c)\\ &= 4x(s-c)\ ;\text{assuming symmetric sea, i.e. } s=\bar s,\ c=\bar c. \end{aligned} \tag{16.6}$$

To extract $F_{2N}^{\rm avg}$ from the cross section measurements (using Eq. (16.5)), ΔxF_{3N} is taken from a NLO QCD model and the input value of the ratio $R_L(x,Q^2)=\frac{\sigma_L(x,Q^2)}{\sigma_T(x,Q^2)}$ is taken from

https://doi.org/10.1017/9781108489065.017 Published online by Cambridge University Press

the empirical fit to the world average data for the electromagnetic induced process (using Eq. (16.3)).

By taking the difference of the neutrino and antineutrino differential scattering cross sections (Eq. (16.4)), one may write:

$$\begin{aligned}\frac{d^2\sigma^{\nu}}{dx\,dy} - \frac{d^2\sigma^{\bar{\nu}}}{dx\,dy} &= \frac{G_F^2 s}{2\pi}\left[\left(1 - y - \frac{Mxy}{2E_l} + \frac{y^2}{2}\frac{1 + 4M^2x^2/Q^2}{1 + R_L}\right)\Delta F_{2N}\right. \\ &+ \left.\left(y - \frac{y^2}{2}\right) xF_{3N}^{\text{avg}}(x, Q^2)\right], \end{aligned} \tag{16.7}$$

where $xF_{3N}^{\text{avg}}(x, Q^2) = \frac{1}{2}[xF_{3N}^{\nu} + xF_{3N}^{\bar{\nu}}]$ and the difference ΔF_{2N} is given by [566]

$$\begin{aligned}\Delta F_{2N} &= F_{2N}^{\nu} - F_{2N}^{\bar{\nu}} = 2(s - \bar{s} + \bar{c} - c) \\ &= 0\,; \quad \text{when symmetric sea is assumed.} \end{aligned} \tag{16.8}$$

ΔF_{2N} is almost negligible, therefore, Eq. (16.4) will have only the average of parity violating structure functions, that is,

$$\frac{d^2\sigma^{\nu}}{dx\,dy} - \frac{d^2\sigma^{\bar{\nu}}}{dx\,dy} = \frac{G_F^2 s}{2\pi}\left[y - \frac{y^2}{2}\right]\left[xF_{3N}^{\text{avg}}(x, Q^2)\right] \tag{16.9}$$

From the cross section measurements, using Eq. (16.9), $xF_{3N}^{\text{avg}}(x, Q^2)$ is obtained.

Hence, by using $l^{\pm}$ and $\nu_l/\bar{\nu}_l$ cross sections measurements, one may extract the structure functions following the methods described earlier.

16.4 Phenomenological Study

Various attempts have been made to understand the nuclear medium effects phenomenologically [814, 815, 816, 817, 818, 819, 820, 821]. Such studies have been made to obtain a nuclear correction factor by doing the analysis of the experimental data on EMC effect from the charged lepton–nucleus scattering, (anti)neutrino–nucleus scattering, and Drell–Yan processes from pion–nucleus scattering, and proton–nucleus scattering. The DIS region has been explored by using the charged lepton beam and the (anti)neutrino beam via the scattering experiments. Neutrinos have an edge over the charged lepton because of their ability to interact with particular quark flavors which would help to understand the partons distribution inside the target nucleon. Another important aspect is that nuclear medium modifications for the weak structure functions may be different from the electromagnetic structure function [822]. The early pioneers in these studies were the experiments with the bubble chambers (BC) led by the Gargamelle heavy liquid bubble chamber (normal filling of CF_3Br). This was followed by the experiments with the smaller ANL and BNL BC as well as the much larger BEBC at CERN and the 15' BC at FNAL filled with hydrogen, deuterium as well as various heavier nuclei such as Ne and propane. With the ANL, BNL, BEBC, and the 15' BC, the use of proton and deuterium targets offered an ideal tool to probe the structure of the free nucleon via the flavor separation offered by the weak charged current. However, the overall statistics was quite limited and

https://doi.org/10.1017/9781108489065.017 Published online by Cambridge University Press

insufficient. The first higher statistics ν and $\bar{\nu}$ nucleus measurements were performed by massive nuclear target detectors like CDHS(W)–iron and CHARM/CHARM II–marble/glass. These early experiments were followed by the CCFR and NuTeV–iron experiments and the CHORUS–lead experiments. As opposed to the high resolution of the earlier low statistics bubble chamber experiments, most of these experimental measurements from heavy nuclear targets could not resolve details of the hadronic shower and concentrated on the inclusive ν and $\bar{\nu}$ cross section measurements [608].

The goal of combining many DIS experimental results on heavy nuclei ranging from ^{12}C to ^{208}Pb was not considered to be a problem if the PDFs (parton distribution function) of the nucleons bound inside the nucleus were assumed to be the same as the free nucleon PDFs. But after the discovery of the EMC effect, it was realized that due to the nuclear environment, the structure functions of a bound nucleon are different from the free nucleon structure functions (see Figure 16.2). Currently, the analyses of both free and bound nucleons are based on the same factorization theorems [823, 824] used in the case of nucleons that do not in any way consider the nuclear environment. However, the nuclear PDFs must account for the nuclear medium effects like shadowing, antishadowing, and the EMC effect at the leading twist. The PDFs of a free proton are well studied with several global analyses being regularly updated [825]. The partonic structure of the bound nucleons must reflect the nuclear environment and, consequently, the nucleus cannot simply be considered as an ensemble of Z free protons PDFs and (A–Z) free neutron PDFs. Nuclear PDFs have been determined by several groups [817, 816, 826, 815] using global fits to experimental data that include, mainly, deep inelastic scattering and Drell–Yan lepton pair production on nuclei.

In the phenomenological analyses of structure functions, the general approach is that these nuclear PDFs are obtained using the charged lepton–nucleus scattering data. The ratios of the structure functions, for example, $\frac{F_{2A}}{F_{2A'}}$, $\frac{F_{2A}}{F_{2D}}$ are analyzed, where A, A' represent any two nuclei and D stands for the deuteron, to determine the nuclear correction factor $R_i(x, Q, A)$. The nuclear correction factor is then multiplied with free nucleon PDFs to get nuclear PDFs, that is,

$$f_i^{(p/A)}(x, Q) = R_i(x, Q, A) f_i^{\text{free proton}}(x, Q).$$

While determining the nuclear correction factor, the information regarding nuclear modification is also obtained from the Drell–Yan cross section ratio like $\frac{\sigma_{pA}^{DY}}{\sigma_{pD}^{DY}}$, $\frac{\sigma_{pA}^{DY}}{\sigma_{pA'}^{DY}}$, where p stands for proton beam. Furthermore, the information about the nuclear correction factor is also supplemented by high energy reaction data from the experiments at LHC, RHIC, etc. This approach has been used by Hirai et al. [815], Eskola et al. [816], Bodek and Yang [827], de Florian and Sassot [817], and others (Table 16.2). The same nuclear correction factor is taken for the weak DIS processes. In a recent analysis, de Florian et al. [817] have analyzed ν-A DIS data, and the data from charged lepton-nucleus scattering and Drell-Yan processes. Their [817] conclusion is that the same nuclear correction factor can describe the nuclear medium effect in $l^{\pm}$-A and ν-A DIS processes.

In another approach, nuclear PDFs are directly obtained by analyzing the experimental data, that is, without using nucleon PDFs or the nuclear correction factor. This approach has

https://doi.org/10.1017/9781108489065.017 Published online by Cambridge University Press

Table 16.2 The developments in the global DGLAP analysis of nPDFs since 1998. DIS: deep inelastic scattering; DY: Drell–Yan di-lepton production; nFFs: nuclear fragmentation functions.

Phenomenological group	Data types used
EKS98 [828, 829]	l+A DIS, p+A DY
HKM [830]	l+A DIS
HKN04 [831]	l+A DIS, p+A DY
nDS [814]	l+A DIS, p+A DY
EKPS [832]	l+A DIS, p+A DY
HKN07 [815]	l+A DIS, p+A DY
EPS08 [833]	l+A DIS, p+A DY, $h^{\pm}$, π^0, $\pi^{\pm}$ in d+Au
EPS09 [816]	l+A DIS, p+A DY, π^0 in d+Au
nCTEQ [826, 834]	l+A DIS, p+A DY
nCTEQ [835]	l+A and ν+A DIS, p+A DY
DSSZ [817]	l+A and ν+A DIS, p+A DY,π^0, $\pi^{\pm}$ in d+Au, computed with nFFs

been recently used by the nCTEQ [819, 818] group in getting $F_{2A}^{\rm EM}(x,Q^2)$, $F_{2A}^{\rm WI}(x,Q^2)$, and $F_{3A}^{\rm WI}(x,Q^2)$, by analyzing the charged lepton-A DIS data and DY p-A data sets together, and the $\nu(\bar{\nu})-A$ DIS data sets separately. Their observation is that the nuclear medium effects in $F_{2A}^{\rm EM}(x,Q^2)$ in electromagnetic interactions are different from $F_{2A}^{\rm WI}(x,Q^2)$ in weak interactions in the region of low x. Thus, in this region, there is a disagreement between the observation of de Florian and Sassot [817] and Kovarik et al. [817, 819].

The study of nuclear medium effects due to modifications of sea quark distributions, nuclear shadowing, and mesonic contributions are important in this region.

In the nCTEQ framework, the parton distributions of the nucleus are constructed as:

$$f_i^{(A,Z)}(x,Q)=\frac{Z}{A}f_i^{p/A}(x,Q)+\frac{A-Z}{A}f_i^{n/A}(x,Q), \tag{16.10}$$

where Z is the number of protons and A is the number of protons plus neutrons in the nucleus. Isospin symmetry is used to construct the PDFs of a bound neutron, $f_i^{n/A}(x,Q)$, from those of the proton by exchanging up and down quark distributions.

The parameterization of the individual parton distributions at the input scale Q_0 are similar in form to that used in the free proton CTEQ fits [836], and takes the following form:

$$\begin{aligned} x f_i^{p/A}(x,Q_0) &= c_0\, x^{c_1}(1-x)^{c_2}e^{c_3 x}(1+e^{c_4}x)^{c_5}, \\ &\quad \text{for} \quad i=u_v,d_v,g,\bar{u}+\bar{d},s+\bar{s},s-\bar{s}, \\ \frac{\bar{d}(x,Q_0)}{\bar{u}(x,Q_0)} &= c_0\, x^{c_1}(1-x)^{c_2}+(1+c_3 x)(1-x)^{c_4}. \end{aligned} \tag{16.11}$$

The input scale is chosen to be the same as for the free proton fits [836], namely $Q_0=1.3$ GeV and the DGLAP equation is used to evolve to higher Q. Figure 16.4, shows the A-dependence of the nCTEQ bound proton PDFs at the scale $Q=10$ GeV for a range of nuclei from the free

https://doi.org/10.1017/9781108489065.017 Published online by Cambridge University Press

proton ($A = 1$) to lead ($A = 208$). Large variation in the quark distribution function may be observed when one goes from lighter targets to very heavy nuclear targets.

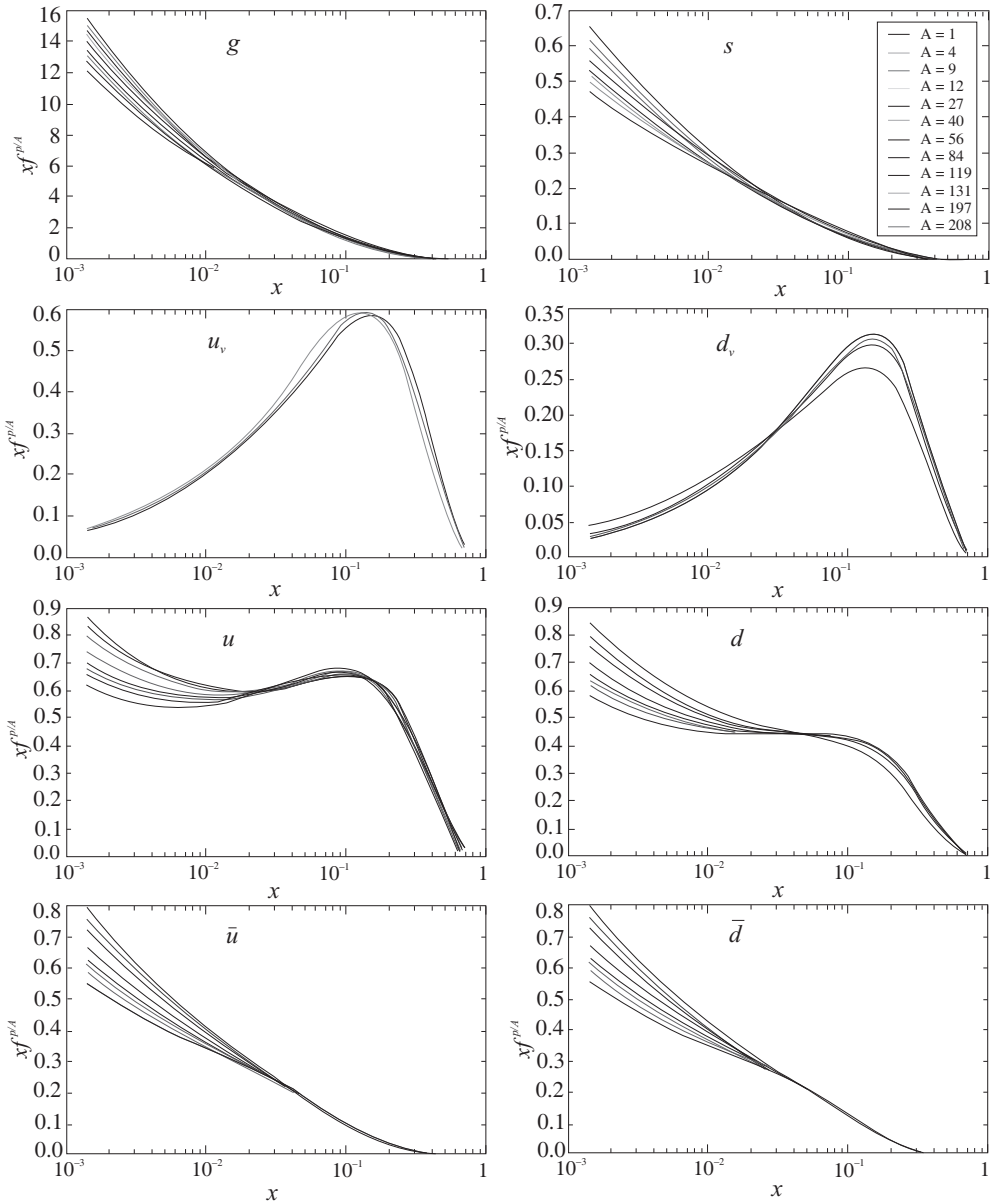

Figure 16.4 The A-dependence of the nCTEQ bound proton PDFs at the scale $Q = 10$ GeV for a range of nuclei from the free proton ($A = 1$) to lead ($A = 208$) [819].

https://doi.org/10.1017/9781108489065.017 Published online by Cambridge University Press

To understand the variation in different phenomenological studies, the nuclear correction factor for the structure function $F_2(x, Q^2)$ in neutrino and antineutrino scattering from ^{56}Fe for $Q^2 = 5$ and 20 GeV^2 has been shown in Figure 16.5. The results are presented from the nCTEQ analysis of NuTeV data [566, 837], the correction factor from HKN07 [815], SLAC/NMC [837] parameterization, and the theoretical work of Kulagin and Petti [800]. The figure has been taken from Ref. [837]. Large variation in the correction factor may be observed.

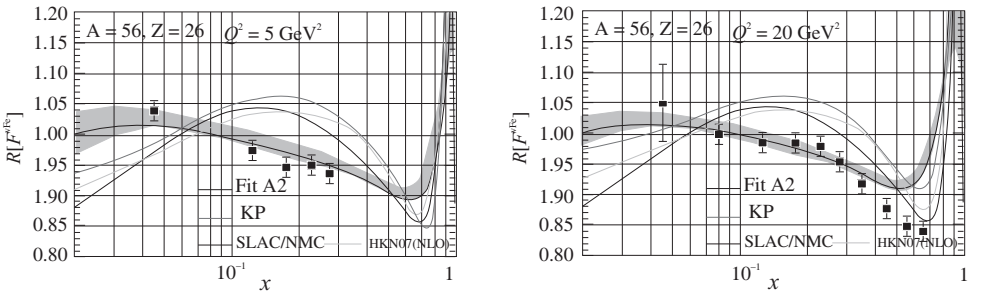

Figure 16.5 Nuclear correction factor R for the structure function F_2 in neutrino and antineutrino scattering from Fe for $Q^2 = 5$ and 20 GeV^2. The solid curve shows the result of the nCTEQ analysis of NuTeV data [566, 837], the uncertainty from the fit is represented by the shaded band. The dashed-double dotted line represents the correction factor from HKN07 [815], the dashed line represents the results for the SLAC/NMC [837] parameterization and the dashed-dotted line represents the results of Kulagin and Petti [800]. The figure has been taken from Ref. [837].

Recently, the MINERvA collaboration [627] has presented their results for the cross section ratios

$$\frac{\left(\frac{d\sigma}{dx}\right)_i}{\left(\frac{d\sigma}{dx}\right)_{CH}}, \quad i = {}^{12}\text{C}, {}^{56}\text{Fe and } {}^{208}\text{Pb; where CH is a hydrocarbon,}$$

as a function of x in several nuclear targets, and compared their data with different phenomenological analysis available in the literature, for example, from GENIE [606] Monte Carlo generator which uses Bodek and Yang parameterization of PDFs [827] and also with the parameterization of Cloet et al. [838]. Bodek and Yang use A-dependent parametrization of the x dependent effects based on charged lepton scattering data and Cloet et al. [838] prescription is based on the convolution of Nambu–Jona–Lasinio nuclear wave function with free nucleon valence PDFs. It may be observed from Figure 16.6 that there is a need to have a better understanding of nuclear effects in the weak interaction induced DIS processes.

In Figure 16.7, the results of differential scattering cross section are presented at neutrino energy of 65 GeV by using the recent nuclear PDFs parameterizations of nCTEQ15 [819] and nCTEQnu [839]. These nuclear PDFs, that is, nCTEQ15 and nCTEQnu are respectively obtained by analyzing the experimental data of charged lepton–nucleus and neutrino–nucleus induced processes. From the figure, it may be observed that the results of charged lepton based nPDFs and neutrino based nPDFs differ from each other in the region of low and high x albeit the difference is small.

https://doi.org/10.1017/9781108489065.017 Published online by Cambridge University Press

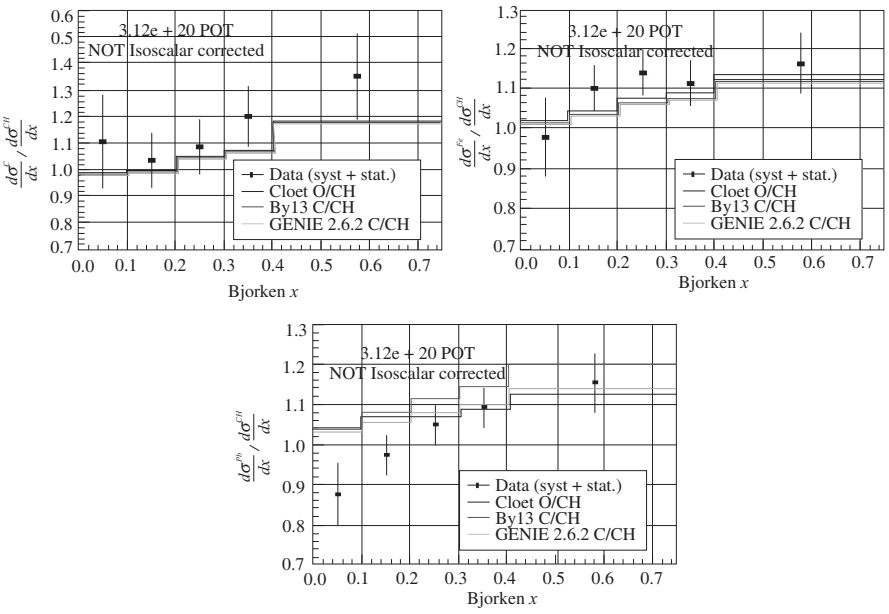

Figure 16.6 DIS cross section ratios as a function of x for MINERvA data points and various parameterizations of x-dependent nuclear effects [606, 827, 838]. The error bars on the data are the combined statistical and systematic uncertainties.

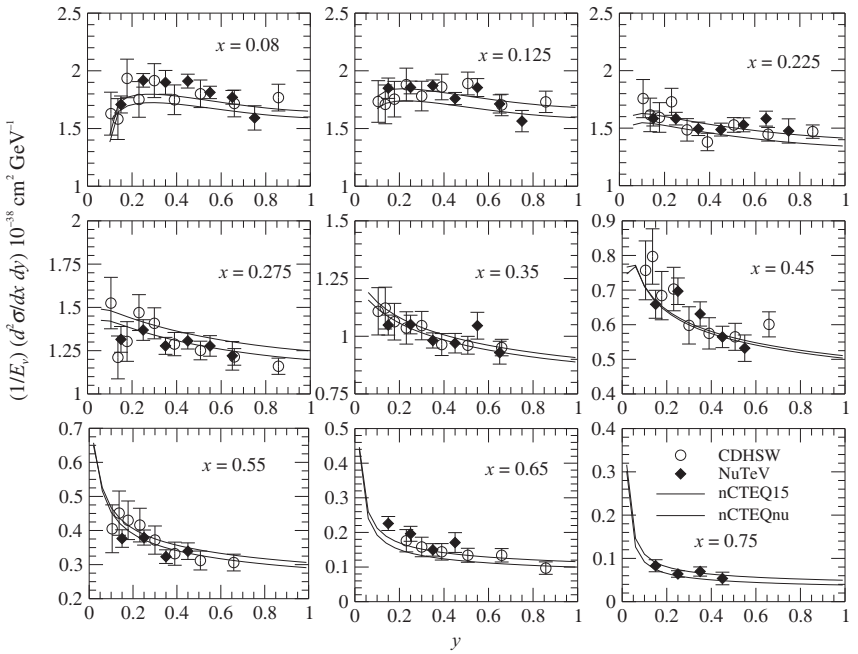

Figure 16.7 Differential scattering cross section $\frac{1}{E_\nu}\frac{d^2\sigma}{dxdy}$ vs. y, at different x for $\nu_\mu - {}^{56}$Fe DIS process at $E_\nu = 65$ GeV [566, 561, 819, 839].

https://doi.org/10.1017/9781108489065.017 Published online by Cambridge University Press

In the next section, different theoretical attempts made to understand the nuclear medium effects are discussed in brief; a field theoretical prescription for taking into account nuclear medium effects which is based on the model developed by the Aligarh–Valencia group is discussed in some detail.

16.5 Theoretical Study

Theoretically, many models have been proposed to study these effects on the basis of nuclear binding, nuclear medium modifications including short range correlations in nuclei [840, 841, 842, 802, 843, 844, 845, 846, 809, 847, 848, 799, 849, 800, 850, 851, 852, 853, 854, 855, 856, 857, 858, 859, 860, 861, 862, 863], pion excess in nuclei [842, 843, 809, 858, 859, 860], multi-quark clusters [861, 862, 863], dynamical rescaling [864, 865], nuclear shadowing [866, 867], etc. In spite of these efforts, no comprehensive theoretical/phenomenological understanding of the nuclear modifications of the bound nucleon structure functions across the complete range of x and Q^2 consistent with the presently available experimental data exists [844, 868, 845, 846].

16.5.1 Deep inelastic charged leptons and (anti)neutrino scattering from nuclei

We have defined the cross sections for the deep inelastic scattering of charged leptons and (anti)neutrinos from nucleon targets in Chapter 13 (see Eqs. (13.18) and (13.63)) in terms of leptonic ($L_{\mu\nu}$) and hadronic ($W_N^{\mu\nu}$) tensors. In a similar way, we define the cross sections for the DIS charged lepton and charged current (anti)neutrino scattering from nuclear targets, that is, $\frac{d^2\sigma^{l^\pm}}{d\Omega_l' dE_l'}$ and $\frac{d^2\sigma_N^{\nu(\bar{\nu})}}{d\Omega_l' dE_l'}$.

$$\frac{d^2\sigma_A^j}{d\Omega_l' dE_l'} \;=\; C_j \times \frac{|\vec{k}'|}{|\vec{k}|}\, L^j_{\mu\nu}\, W^{\mu\nu}_{A,j}, \tag{16.12}$$

where j stands for either the electromagnetic or weak interaction channel and the constant factor $C_j = \frac{\alpha^2}{Q^4}$ for the electromagnetic interaction and $C_j = \frac{G_F^2}{(2\pi)^2}\left(\frac{M_W^2}{M_W^2+Q^2}\right)^2$ for the weak interaction induced processes. $L^j_{\mu\nu}$ is the leptonic tensor as given in Eqs. (13.4) and (13.60) for the corresponding interaction channels. $W^{\mu\nu}_{A,j}$ is the nuclear hadronic tensor which is written in terms of the nuclear structure functions as:

$$W^{\mu\nu}_{A,WI} = \left(\frac{q^\mu q^\nu}{q^2} - g^{\mu\nu}\right) W_{1A}^{\rm WI}(\nu, Q^2) + \frac{W_{2A}^{\rm WI}(\nu, Q^2)}{M_A^2}\left(p_A^\mu - \frac{p_A.q}{q^2}\, q^\mu\right)\left(p_A^\nu - \frac{p_A.q}{q^2}\, q^\nu\right) - \frac{i}{2M_A^2}\epsilon^{\mu\nu\rho\sigma} p_{A\rho} q_\sigma\, W_{3A}^{\rm WI}(\nu, Q^2). \tag{16.13}$$

https://doi.org/10.1017/9781108489065.017 Published online by Cambridge University Press

for the (anti)neutrino induced processes that deal with the parity violation. For the charged lepton induced processes, it is given in terms of only two nuclear structure functions

$$W^{\mu\nu}_{A,EM} = \left(\frac{q^\mu q^\nu}{q^2} - g^{\mu\nu}\right) W^{\rm EM}_{1A}(\nu, Q^2) + \left(p^\mu_A - \frac{p_A.q}{q^2}\, q^\mu\right)\left(p^\nu_A - \frac{p_A.q}{q^2}\, q^\nu\right)\frac{W^{\rm EM}_{2A}(\nu, Q^2)}{M^2_A}, \tag{16.14}$$

because $W_{3A}(\nu, Q^2) = 0$ due to parity invariance. The contraction of leptonic and hadronic tensors simplifies the expression of differential scattering cross section to the following forms:

$$\frac{d^2\sigma^{\rm WI}_A}{d\Omega'_l dE'_l} = \frac{G^2_F E'^2_l}{2\pi^2}\left(\frac{M^2_W}{M^2_W + Q^2}\right)^2 \left[2W^{\rm WI}_{1A}(\nu, Q^2)\sin^2\frac{\theta}{2} + W^{\rm WI}_{2A}(\nu, Q^2)\cos^2\frac{\theta}{2} \pm W^{\rm WI}_{3A}(\nu, Q^2)\left(\frac{E_l + E'_l}{M_A}\right)\sin^2\frac{\theta}{2}\right], \tag{16.15}$$

and

$$\frac{d^2\sigma^{\rm EM}_A}{d\Omega'_l dE'_l} = \frac{4\alpha^2 E'^2_l}{Q^4}\left[2W^{\rm EM}_{1A}(\nu, Q^2)\sin^2\frac{\theta}{2} + W^{\rm EM}_{2A}(\nu, Q^2)\cos^2\frac{\theta}{2}\right]. \tag{16.16}$$

In Eq. (16.15), the positive sign is for the neutrino and the negative sign is for the antineutrino induced process.

The weak nuclear structure functions $W^{WI}_{iA}(\nu, Q^2)$ $(i = 1, 2, 3)$, are defined in terms of the dimensionless nuclear structure functions $F^{WI}_{iA}(x, Q^2)$ as:

$$\left.\begin{array}{l} M_A W^{WI}_{1A}(\nu_A, Q^2) = F^{WI}_{1A}(x_A, Q^2), \\ \nu_A W^{WI}_{2A}(\nu_A, Q^2) = F^{WI}_{2A}(x_A, Q^2), \\ \nu_A W^{WI}_{3A}(\nu_A, Q^2) = F^{WI}_{3A}(x_A, Q^2), \end{array}\right\} \tag{16.17}$$

where the energy transfer $\nu_A = \frac{p_A \cdot q}{M_A} = q^0$.

In Subsection 16.5.1, a general idea of nuclear medium effects such as Fermi motion, Pauli blocking, and nuclear binding of nucleons is discussed in brief.

Nuclear binding, Pauli blocking, and Fermi motion of nucleons

The general approach to calculate the DIS cross section is based on an impulse approximation in which the nuclear cross section is the incoherent sum of scattering from neutrons and protons. Additional contribution due to off-shell effects and other degrees of freedom like mesons, resonances, quark clusters, or gluons are calculated as corrections. In this approach, the DIS process is considered as a two-step process, in which $W^{\pm}(Z^0)$ bosons or virtual photons scatter from the partons in the bound hadrons in the nucleus, that is, nucleons, mesons, etc. described by the structure function of the hadron and then convoluted with the momentum distribution of struck hadrons inside the nucleus. The effect of nuclear binding and Fermi motion and the nucleon–nucleon correlation can be included in the momentum distribution, described by the spectral function of nucleons, or the Fermi smearing function in the momentum space

https://doi.org/10.1017/9781108489065.017 Published online by Cambridge University Press

depending upon what nuclear effects are included in deriving the spectral functions. In this approach, the nuclear structure functions ($F_i^A(x, Q^2)$) can be formally written as:

$$F_i^A(x, Q^2) = \sum_C \int \frac{d^4p}{(2\pi)^4} S_C(E, \vec{p}) F_i^C(x, Q^2, p), \tag{16.18}$$

where $i = 1, 2$ in the case of charged lepton and $i = 1, 2, 3$ in case of (anti)neutrino DIS from nucleons. In Eq. (16.18), the summation is performed over the cluster C which could be protons, neutrons, mesons like π and ρ or quark clusters. $S_C(E, \vec{p})$ is the spectral function of the cluster C, with energy E and momentum $\vec{p}$ in the nucleus. The integration is performed over all the possible momenta of the cluster subject to the energy momentum conservation of the cluster inside the nucleus. Explicit expressions for the nuclear structure functions $F_i^A(x, Q^2)$ are derived starting from the relation between the nuclear hadronic tensor $W_{\mu\nu}^A(x, Q^2)$ and nucleon hadronic tensor $W_{\mu\nu}^N(x, Q^2)$ for electromagnetic and weak interactions, which will be discussed later in the text.

Over the last 35 years, there have been various models proposed to calculate nuclear structure functions. It is not possible to describe all of them here and our present discussions will be limited to two models which have been recently used to study the nuclear medium effects in neutrino and antineutrino scattering from nuclear targets. First, we shall discuss the Aligarh–Valencia model [809, 850, 851, 852, 854, 855, 869, 822, 870, 871] and then, in brief, the Kulagin and Petti model [800, 799].

16.5.2 Aligarh–Valencia model

In this model, the nuclear hadronic tensor $W_{\mu\nu}^A$ is evaluated using local density approximation. To calculate the scattering cross section for a neutrino interacting with a target nucleon in the nuclear medium, we start with a flux of neutrinos hitting a collection of target nucleons over a given length of time. A majority of neutrinos will simply pass through the target without interacting while a certain fraction will interact with the target nucleons leaving the pass-through fraction and entering the fraction of neutrinos yielding final state leptons and hadrons. Here, we will introduce the concept of 'neutrino self-energy' that has a real and imaginary part. The real part modifies the lepton mass (it is similar to the delta mass or nucleon mass modified in the nuclear medium), while the imaginary part is related to this fraction of interacting neutrinos and gives the total number of neutrinos that have participated in the interactions that give rise to the charged leptons and hadrons. When a neutrino interacts with a potential provided by a nucleus (in the present scenario), then the interaction in the language of many body field theory, can be understood as the modification of the fermion two points function represented by the diagrams shown in Figure 16.8.

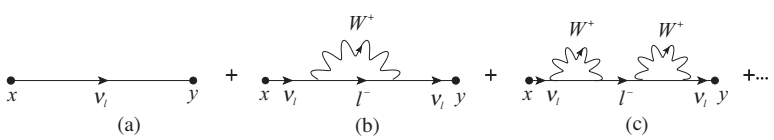

Figure 16.8 Representation of neutrino self-energy.

https://doi.org/10.1017/9781108489065.017 Published online by Cambridge University Press

The first diagram (a) in Figure 16.8 is just the free field fermion propagator. The diagrams, Figure 16.8 (b) and (c) contribute to the neutrino self-energy in the lowest order and higher order (Chapter 4), respectively. Using the Feynman rules, the self energy $\Sigma(k)$ in the lowest order may be written as (Figure 16.9):

$$-i\Sigma(k) = \sum_{\text{spins}} \int \frac{d^4k'}{(2\pi)^4} \left(-\frac{ig}{2\sqrt{2}}\gamma^\mu(1-\gamma_5)\right) \frac{i(\not{k}' + m_l)}{k'^2 - m_l^2 + i\epsilon} \times \left(-\frac{ig}{2\sqrt{2}}\gamma^\nu(1-\gamma_5)\right) \frac{-ig_{\mu\nu}}{(k-k')^2 - M_W^2 + i\epsilon}. \tag{16.19}$$

Notice that Σ has real and imaginary parts. The imaginary part of the neutrino self-energy accounts for the depletion of the initial neutrinos flux out of the non-interacting channel, into the quasielastic or the inelastic channels.

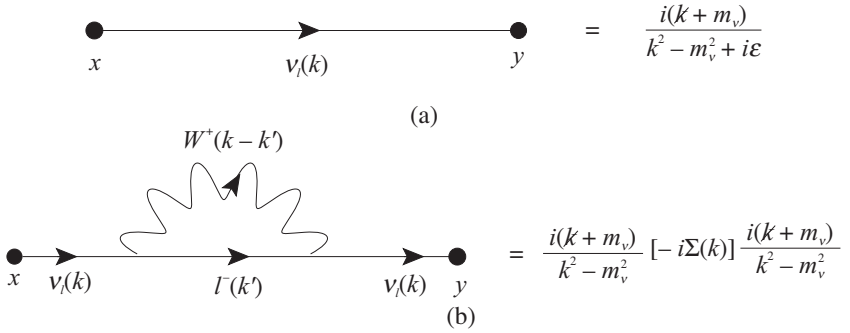

Figure 16.9 (a) Free field fermion propagator. (b) The term that contributes to the neutrino self-energy in the lowest order.

When the neutrinos interact with the nucleus, the virtual W^+ in Figure 16.9, creates particle–hole (p,h) excitations of the type $(1p, 1h)$, $(1\Delta, 1h)$, ... or (X, h) leading to quasielastic, inelastic Δ production or DIS with production of a set of particles X. The (X, h) excitations as shown in Figure 16.10 give rise to reactions like $\nu_l(\bar{\nu}_l) + A \rightarrow l^-(l^+) + X$. The neutrino self-energy is then evaluated corresponding to the diagram shown in Figure 16.10. The cross section for an element of volume dV in the rest frame of the nucleus is related to the probability per unit time (Γ) of the ν_l interacting with a nucleon bound inside a nucleus. The quantity $\Gamma dt dS$ provides probability times a differential of area (dS) which is nothing but the cross section ($d\sigma$) [809], that is,

$$d\sigma = \Gamma dt ds = \Gamma \frac{dt}{dl} ds dl = \Gamma \frac{1}{v} dV = \Gamma \frac{E_l}{|\vec{k}|} d^3r, \tag{16.20}$$

where $v \left(= \frac{|\vec{k}|}{E_l}\right)$ is the velocity of the incoming ν_l. The probability per unit time of the interaction of ν_l with the nucleons in the nuclear medium to give the final state is related to the imaginary part of the ν_l self-energy as [809]:

https://doi.org/10.1017/9781108489065.017 Published online by Cambridge University Press

$$-\frac{\Gamma}{2} = \frac{m_\nu}{E_\nu(\vec{k})}\,\mathrm{Im}\Sigma(k), \tag{16.21}$$

where $\Sigma(k)$ is the neutrino self-energy (shown in Figure 16.10 (a) and (b)). By using Eq. (16.21) in Eq. (16.20), we obtain:

$$d\sigma = \frac{-2m_\nu}{|\vec{k}|}\mathrm{Im}\Sigma(k)d^3r. \tag{16.22}$$

$\Sigma(k)$ is calculated from Figure 16.10, that is,

$$\Sigma(k) \;=\; \frac{iG_F}{\sqrt{2}}\int\frac{d^4q}{(2\pi)^4}\frac{4L^{\mathrm{WI}}_{\mu\nu}}{m_l}\frac{1}{(k'^2-m_l^2+i\epsilon)}\left(\frac{M_W}{q^2-M_W^2}\right)^2\Pi^{\mu\nu}(q)\,, \tag{16.23}$$

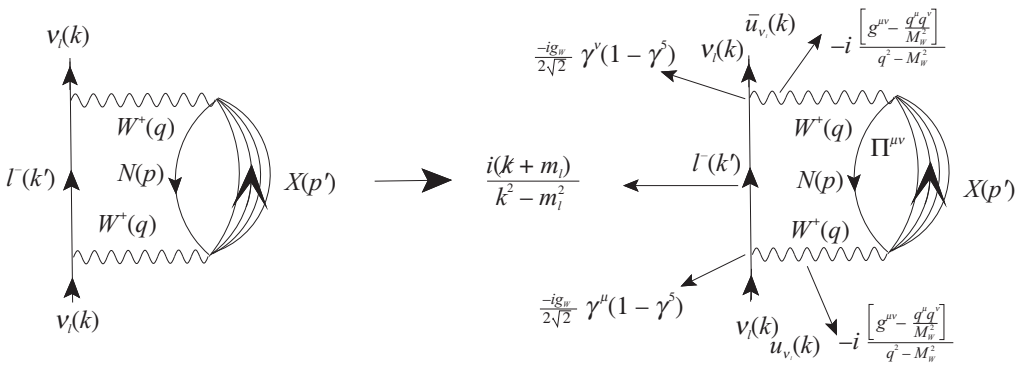

Figure 16.10 Diagrammatic representation of the neutrino self-energy.

where we have used the relation $\frac{g_W^2}{8M_W^2} = \frac{G_F}{\sqrt{2}}$ and the properties of gamma matrices. The imaginary part of the neutrino self-energy may be obtained by following the Cutkowsky rules [872] as:

$$\mathrm{Im}\Sigma(k) = \frac{G_F}{\sqrt{2}}\frac{4}{m_\nu}\int\frac{d^4k'}{(2\pi)^4}\frac{\pi}{E(\vec{k}')}\theta(q^0)\left(\frac{M_W}{Q^2+M_W^2}\right)^2\mathrm{Im}\left[L_{\mu\nu}\Pi^{\mu\nu}(q)\right]. \tag{16.24}$$

In this expression, $\Pi^{\mu\nu}(q)$ is the W boson self-energy, which is written in terms of the nucleon (G_l) and meson (D_j) propagators (depicted in Figure 16.11) following the Feynman rules and is given by:

$$\Pi^{\mu\nu}(q) \;=\; \left(\frac{G_F M_W^2}{\sqrt{2}}\right)\times\int\frac{d^4p}{(2\pi)^4}G(p)\sum_X\sum_{s_p,s_l}\prod_{i=1}^{N}\int\frac{d^4p_i'}{(2\pi)^4}\prod_l G_l(p_l')\prod_j D_j(p_j')$$
$$\langle X|J^\mu|N\rangle\langle X|J^\nu|N\rangle^*(2\pi)^4\,\delta^4(k+p-k'-\sum_{i=1}^{N}p_i'), \tag{16.25}$$

https://doi.org/10.1017/9781108489065.017 Published online by Cambridge University Press

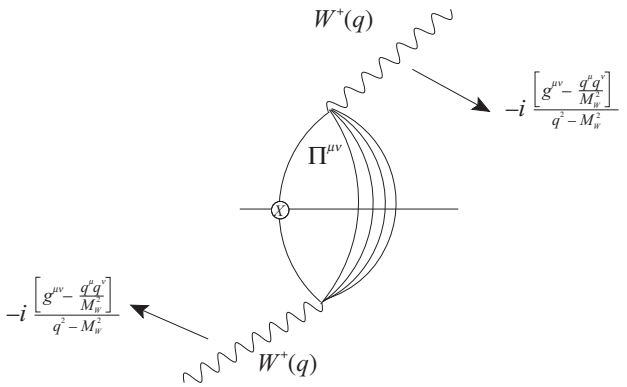

Figure 16.11 Diagrammatic representation of intermediate vector boson W self-energy.

where s_p is the spin of the nucleon, s_l is the spin of the fermions in X, $\langle X|J^\mu|N\rangle$ is the hadronic current for the initial state nucleon to the final state hadrons, index l, j are respectively, stands for the fermions and for the bosons in the final hadronic state X, and $\delta^4(k+p-k'-\sum_{i=1}^{N} p_i')$ ensures the conservation of four momentum at the vertex. The nucleon propagator $G(p)$ inside the nuclear medium provides information about the propagation of the nucleon from the initial state to the final state or vice versa.

The relativistic nucleon propagator $G(p^0,\vec{p})$ in a nuclear medium is obtained by starting with the relativistic free nucleon Dirac propagator $G^0(p^0,\vec{p})$, which is written in terms of the contribution from the positive and negative energy components of the nucleon described by the Dirac spinors $u(\vec{p})$ and $v(\vec{p})$ [801, 809]. Only the positive energy contributions are retained as the negative energy contributions are suppressed. In the interacting Fermi sea, the relativistic nucleon propagator is then written in terms of the nucleon self-energy $\Sigma^N(p^0,\vec{p})$ which is shown in Figure 16.12. In the nuclear many body technique, the quantity that contains all the information on single nucleon properties in the nuclear medium is the nucleon self-energy $\Sigma^N(p^0,\vec{p})$. For an interacting Fermi sea, the relativistic nucleon propagator is written in terms of the nucleon self-energy and in nuclear matter, the interaction is taken into account through Dyson series expansion. The Dyson series expansion may be understood as the quantum field theoretical analog of the Lippmann–Schwinger equation for the dressed nucleons, which is in principle an infinite series in perturbation theory. This perturbative expansion is summed in a ladder approximation and we will now illustrate the methods.

Let us start with the expression of relativistic free nucleon Dirac propagator $G^0(p)$ given by

$$G^0(p) = \frac{1}{\not{p} - M + i\epsilon} = \frac{\not{p} + M}{(p^2 - M^2 + i\epsilon)} \tag{16.26}$$

which may be rewritten in terms of positive and negative energy states as:

$$G^0(p) = \frac{M}{E_N(\vec{p})}\left\{\frac{\sum_r u_r(\vec{p})\bar{u}_r(\vec{p})}{p^0 - E_N(\vec{p}) + i\epsilon} + \frac{\sum_r v_r(-\vec{p})\bar{v}_r(-\vec{p})}{p^0 + E_N(\vec{p}) - i\epsilon}\right\}, \tag{16.27}$$

https://doi.org/10.1017/9781108489065.017 Published online by Cambridge University Press

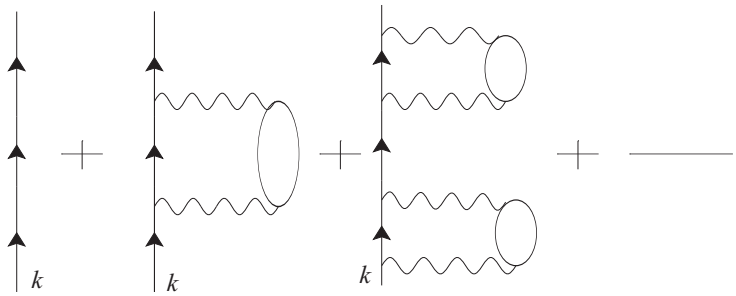

Figure 16.12 Diagrammatic representation of nucleon self-energy in the nuclear medium.

where $\sum_{r=1}^{2} u_r(\vec{p})\bar{u}_r(\vec{p}) = \frac{\not{p}+M}{2M}$, $\sum_{r=1}^{2} v_r(-\vec{p})\bar{v}_r(-\vec{p}) = \frac{\not{p}-M}{2M}$, M is the nucleon mass, $E_N(\vec{p}) = \sqrt{\vec{p}^2 + M^2}$ is the relativistic energy of an on-shell nucleon, and $\bar{u}_r(\vec{p})\ u_r(\vec{p}) = 1$. Notice that we are using a different normalization than the one discussed in Chapter 2. This has been chosen for convenience.

The Dirac propagator in a non-interacting Fermi sea may also be written as

$$G^0(p) = \frac{M}{E_N(\vec{p})}\left\{\sum_r u_r(\vec{p})\bar{u}_r(\vec{p})\left[\frac{1-n(\vec{p})}{p^0 - E_N(\vec{p}) + i\epsilon} + \frac{n(\vec{p})}{p^0 - E_N(\vec{p}) - i\epsilon}\right] + \frac{\sum_r v_r(-\vec{p})\bar{v}_r(-\vec{p})}{p^0 + E_N(\vec{p}) - i\epsilon}\right\}, \tag{16.28}$$

where $n(\vec{p})$ is the occupation number of a nucleon lying within the Fermi sea such that

$$n(\vec{p}) = \begin{cases} 1 & \text{for } \vec{p} \le \vec{p}_{F_N} \\ 0 & \text{for } \vec{p} > \vec{p}_{F_N} \end{cases} \tag{16.29}$$

with $\vec{p}_{F_N}$ as the Fermi momentum of the nucleon.

The nucleon propagator retains the contribution only from the positive energy components because the negative energy components are much suppressed. Hence, Eq. (16.28) reduces to

$$G^0(p) = \frac{M}{E_N(\vec{p})}\sum_r u_r(\vec{p})\bar{u}_r(\vec{p})\left[\frac{1-n(\vec{p})}{p^0 - E_N(\vec{p}) + i\epsilon} + \frac{n(\vec{p})}{p^0 - E_N(\vec{p}) - i\epsilon}\right]. \tag{16.30}$$

The first term of the nucleon propagator within the square bracket contributes when the momentum of the nucleon will be greater or equal to the Fermi momentum $\vec{p} \ge \vec{p}_F$, that is, for the particles above the Fermi sea while the second term within the square bracket contributes when the nucleon momentum will be less than the Fermi momentum $\vec{p} < \vec{p}_F$, that is, for the particles below the Fermi sea. This representation is known as the Lehmann's representation. With further simplification of Eq. (16.30), we may write:

$$G^0(p) = \frac{\not{p} + M}{p^2 - M^2 + i\epsilon} + 2\,i\pi\theta(p^0)\delta(p^2 - M^2)n(\vec{p})(\not{p} + M). \tag{16.31}$$

https://doi.org/10.1017/9781108489065.017 Published online by Cambridge University Press

Inside the Fermi sea, where nucleons interact with each other, the relativistic nucleon propagator is written by using the Dyson series expansion in terms of the nucleon self-energy $\Sigma^N(p)$ (depicted in Figure 16.12) as:

$$G(p) \;=\; G^0(p) + G^0(p)\Sigma^N(p)G^0(p) + G^0(p)\Sigma^N(p)G^0(p)\Sigma^N(p)G^0(p) + \ldots . \quad (16.32)$$

By using Eq. (16.31) in Eq. (16.32), we obtain a geometric progression series and with further simplification get:

$$\begin{aligned} G(p) &= \frac{M_N}{E(\vec{p})}\frac{\sum_r u_r(\vec{p})\bar{u}_r(\vec{p})}{p^0 - E(\vec{p})} + \frac{M_N}{E(\vec{p})}\frac{\sum_r u_r(\vec{p})\bar{u}_r(\vec{p})}{p^0 - E(\vec{p})}\Sigma^N(p^0,\vec{p})\frac{M_N}{E(\vec{p})}\frac{\sum_r u_r(\vec{p})\bar{u}_r(\vec{p})}{p^0 - E(\vec{p})} + \ldots \\ &= \frac{M_N}{E(\vec{p})}\frac{\sum_r u_r(\vec{p})\bar{u}_r(\vec{p})}{p^0 - E(\vec{p}) - \Sigma^N(p^0,\vec{p})\frac{M_N}{E(\vec{p})}}. \end{aligned} \quad (16.33)$$

Notice that $\Sigma^N(p^0,\vec{p})$ has a finite imaginary part, and therefore, we may write:

$$\Sigma^N(p^0,\vec{p}) = \mathrm{Re}\{\Sigma^N(p^0,\vec{p})\} \;+\; i\mathrm{Im}\{\Sigma^N(p^0,\vec{p})\}. \quad (16.34)$$

The real part of the self-energy is related to the effective mass while the imaginary part is related to the lifetime of the particle ($\mathrm{Im}\Sigma^N = \frac{1}{\tau} = \Gamma$) which allows us to write Eq. (16.33) as:

$$G(p) = \frac{M}{E_N(\vec{p})}\sum_r u_r(\vec{p})\bar{u}_r(\vec{p})\left[\frac{\{p^0 - E_N(\vec{p}) - \frac{M}{E_N(\vec{p})}\mathrm{Re}(\Sigma^N)\} + i\{\frac{M}{E_N(\vec{p})}\mathrm{Im}(\Sigma^N)\}}{\{p^0 - E_N(\vec{p}) - \frac{M}{E_N(\vec{p})}\mathrm{Re}(\Sigma^N)\}^2 + \{\frac{M}{E_N(\vec{p})}\mathrm{Im}(\Sigma^N)\}^2}\right]. \quad (16.35)$$

The nucleon self-energy $\Sigma^N(p^0,\vec{p})$ is spin diagonal, that is, $\Sigma^N_{\alpha\beta}(p^0,\vec{p}) = \Sigma^N(p^0,\vec{p})\delta_{\alpha\beta}$, where α and β are spinorial indices. The inputs required for the NN interaction are incorporated by relating them to the experimental elastic NN cross section. Furthermore, the RPA-correlation effect (described in Chapter 14) is taken into account using the spin–isospin effective interaction as the dominating part of the particle–hole (ph) interaction. Using the modified expression for the nucleon self-energy, the imaginary part of it is obtained. Due to the RPA effect, the imaginary part of the nucleon self-energy is quenched, especially at low energies and high densities. This quenching depends on the nucleon energy p^0 as well as nucleon momentum $\vec{p}$ in the interacting Fermi sea. The imaginary part of the nucleon self-energy fulfills the low-density theorem.

The dressed nucleon propagator $G(p)$ in a nuclear medium is then expressed as [809]:

$$G(p) = \frac{M}{E_N(\vec{p})}\sum_r u_r(\vec{p})\bar{u}_r(\vec{p})\left[\int_{-\infty}^{\mu} d\omega \frac{S_h(\omega,\vec{p})}{p^0 - \omega - i\epsilon} + \int_{\mu}^{\infty} d\omega \frac{S_p(\omega,\vec{p})}{p^0 - \omega + i\epsilon}\right], \quad (16.36)$$

where chemical potential μ is given by

$$\mu = \frac{p_F^2}{2M} \;+\; \mathrm{Re}\Sigma^N\left[\frac{p_F^2}{2M}, p_F\right].$$

https://doi.org/10.1017/9781108489065.017 Published online by Cambridge University Press

ω is the removal energy, $S_h(\omega, \vec{p})$ and $S_p(\omega, \vec{p})$ are the hole and particle spectral functions, respectively, that allow us to know about the probability distribution of finding a nucleon with removal energy ω and three momentum $\vec{p}$ inside the nucleus. Thus, in the aforementioned expression, $S_h(\omega, \vec{p})\ d\omega$ is basically the joint probability of removing a nucleon from the ground state and $S_p(\omega, \vec{p})\ d\omega$ is the joint probability of adding a nucleon to the ground state of a nucleus. Hence, the momentum distribution of the nucleon in an interacting Fermi sea is given by

$$\begin{aligned} \int_{-\infty}^{\mu} S_h(\omega, \vec{p})\ d\omega &= n_I(\vec{p}), \text{ and} \\ \int_{\mu}^{+\infty} S_p(\omega, \vec{p})\ d\omega &= 1 - n_I(\vec{p}), \end{aligned} \tag{16.37}$$

that leads to the spectral function sum rule:

$$\int_{-\infty}^{\mu} S_h(\omega, \vec{p})\ d\omega\ +\ \int_{\mu}^{+\infty} S_p(\omega, \vec{p})\ d\omega\ =\ 1. \tag{16.38}$$

Applying the Sokhatsky–Weierstrass theorem, that is,

$$\lim_{\epsilon \to 0^+} \left(\frac{1}{x \pm i\epsilon} \right) = \mathcal{P}\left(\frac{1}{x} \right) \mp i\pi\delta(x) \tag{16.39}$$

on Eq. (16.36) and then comparing the imaginary part of the obtained expression with Eq. (16.35), we obtain the expressions for the hole and particle spectral functions which are given by [809, 801]:

$$S_h(p^0, \vec{p}) = \frac{1}{\pi} \frac{\frac{M}{E_N(\vec{p})} \mathrm{Im}\Sigma^N(p^0, \vec{p})}{\left(p^0 - E_N(\vec{p}) - \frac{M}{E_N(\vec{p})} \mathrm{Re}\Sigma^N(p^0, \vec{p}) \right)^2 + \left(\frac{M}{E_N(\vec{p})} \mathrm{Im}\Sigma^N(p^0, \vec{p}) \right)^2} \tag{16.40}$$

when $p^0 \leq \mu$,

$$S_p(p^0, \vec{p}) = -\frac{1}{\pi} \frac{\frac{M}{E_N(\vec{p})} \mathrm{Im}\Sigma^N(p^0, \vec{p})}{\left(p^0 - E_N(\vec{p}) - \frac{M}{E_N(\vec{p})} \mathrm{Re}\Sigma^N(p^0, \vec{p}) \right)^2 + \left(\frac{M}{E_N(\vec{p})} \mathrm{Im}\Sigma^N(p^0, \vec{p}) \right)^2} \tag{16.41}$$

when $p^0 > \mu$. With these theoretical inputs, one is prepared to write the cross section by using Eqs. (16.22) and (16.24) in terms of the imaginary part of the W boson self-energy as:

$$\frac{d^2\sigma_A^{WI}}{d\Omega' dE_l'} = -\frac{G_F^2}{(2\pi)^2} \frac{|\vec{k}'|}{|\vec{k}|} \left(\frac{M_W^2}{M_W^2 + Q^2} \right)^2 \int Im(L_{\mu\nu} \Pi^{\mu\nu}) d^3r. \tag{16.42}$$

https://doi.org/10.1017/9781108489065.017 Published online by Cambridge University Press

The hadronic tensor $W_A^{\mu\nu}$ is now given by

$$W_A^{\mu\nu} = -\int d^3r \, Im\Pi^{\mu\nu}(q) \tag{16.43}$$

Using Eq. (16.36) and the expressions for the free nucleon and meson propagators in Eq. (16.25), and finally substituting them in Eq. (16.43), we obtain the nuclear hadronic tensor $W_A^{\mu\nu}$ for a nucleus having $N \neq Z$ in terms of the nucleonic hadronic tensor $W_N^{\mu\nu}$ convoluted with the hole spectral function (S_h^τ, $(\tau = p, n)$) for a nucleon bound inside the nucleus:

$$W_A^{\mu\nu} = 2 \sum_{\tau=p,n} \int d^3r \int \frac{d^3p}{(2\pi)^3} \frac{M_N}{E_N(\vec{p})} \int_{-\infty}^{\mu_\tau} dp^0 S_h^\tau(p^0, \vec{p}, \rho^\tau(r)) \, W_N^{\mu\nu}(p, q), \tag{16.44}$$

where factor 2 is due to the two possible spin projections of protons or neutron, $\mu_p(\mu_n)$ is the chemical potential for the proton (neutron). $S_h^p(\omega, \vec{p}, \rho_p(r))$ and $S_h^n(\omega, \vec{p}, \rho_n(r))$ are the hole spectral functions for the proton and neutron, respectively, which provide information about the probability distribution of finding a proton and neutron with removal energy ω and three momentum $\vec{p}$ inside the nucleus. $\rho^\tau(r)$ is the charge density of the proton or neutron and has already been discussed in Chapter 14.

In the local density approximation, Fermi momentum is not fixed but depends upon the interaction point (r) in the nucleus and is bounded by $p_F(r)$ at the point r by

$$p_{F_{p(n)}}(r) = \left(\frac{3\pi^2 \rho_{p(n)}(r)}{2} \right)^{1/3}. \tag{16.45}$$

for the proton (neutron) target. Through the hole spectral function $(S_h(p^0, \vec{p}, \rho(r)))$, the effects of Fermi motion, Pauli blocking, and nucleon correlations are incorporated. The behavior of hole spectral function vs. removal energy $\omega = p^0 - M$ is shown in Figure 16.13 for ^{12}C, ^{40}Ca, ^{56}Fe, ^{118}Sn, and ^{208}Pb. From the figure, it may be noticed that when the nucleon momentum is less than the Fermi momentum, the spectral function has a sharp and narrow distribution similar to the delta function while for $p > p_F$, the distribution has a wide range though it is very small in magnitude. This behavior of the spectral function is different as found in the case of independent particle model. It may be seen from Figure 16.13, that the hole spectral function has a smaller magnitude for heavier nuclear targets because of the enhancement in the probability of interaction among the nucleons. For an isoscalar nuclear target, the spectral function is properly normalized to reproduce the correct baryon number and binding energy for a given nucleus [869]

$$4 \int \frac{d^3p}{(2\pi)^3} \int_{-\infty}^{\mu} S_h(\omega, \vec{p}, p_F(r)) d\omega = \rho(r) \tag{16.46}$$

or equivalently

$$\int d^3r \, 4 \int \frac{d^3p}{(2\pi)^3} \int_{-\infty}^{\mu} S_h(\omega, \vec{p}, p_F(r)) d\omega = A. \tag{16.47}$$

https://doi.org/10.1017/9781108489065.017 Published online by Cambridge University Press

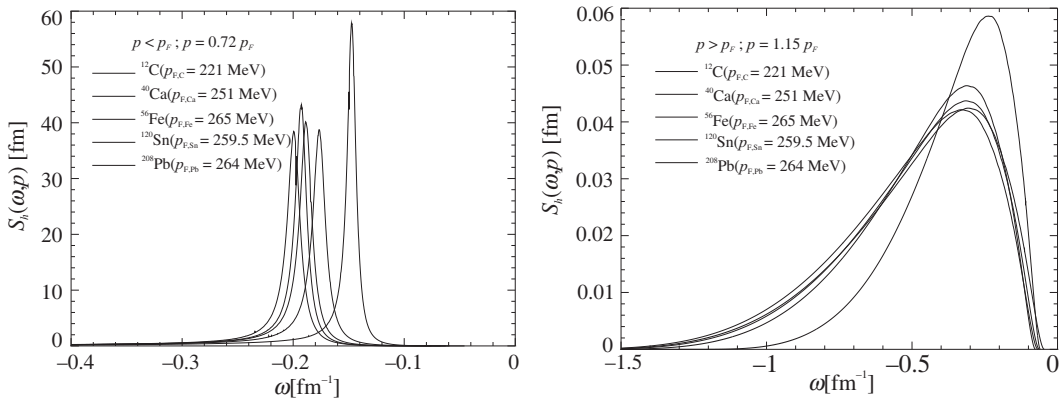

Figure 16.13 Results for $S_h(\omega, \vec{p})$ vs. ω are shown for (a) $p < p_F$ and (b) $p > p_F$ in various nuclei like ^{12}C, ^{40}Ca, ^{56}Fe, ^{120}Sn, and ^{208}Pb.

For a nonisoscalar nuclear target, these spectral functions are normalized individually for the proton (Z) and neutron ($N = A - Z$) numbers, that is,

$$2 \int d^3r \int \frac{d^3p}{(2\pi)^3} \int_{-\infty}^{\mu_p} S_h^p(\omega, \vec{p}, \rho_p(r))\, d\omega = Z\,,$$
$$2 \int d^3r \int \frac{d^3p}{(2\pi)^3} \int_{-\infty}^{\mu_n} S_h^n(\omega, \vec{p}, \rho_n(r))\, d\omega = N.$$

To evaluate the dimensionless nuclear structure functions by using Eq. (16.44), the appropriate components of nucleonic $W_N^{\mu\nu}$ (in Eq. (13.62)) and nuclear $W_A^{\mu\nu}$ (in Eq. (16.13)), hadronic tensors along the X, Y and Z axes are chosen.

By taking the zz component of the hadronic tensors ($W_N^{\mu\nu}$ of Eq. (13.62) and $W_A^{\mu\nu}$ of Eq. (16.13)), for a nonisoscalar nuclear target, the following expression is obtained [852]:

$$F_{2A,N}^{\rm WI}(x_A, Q^2) = 2 \sum_{\tau=p,n} \int d^3r \int \frac{d^3p}{(2\pi)^3} \frac{M_N}{E_N(\vec{p})} \int_{-\infty}^{\mu_\tau} dp^0\, S_h^\tau(p^0, \vec{p}, \rho^\tau(r)) \times \left[\left(\frac{Q}{q^z}\right)^2 \left(\frac{|\vec{p}|^2 - (p^z)^2}{2M_N^2} \right) + \frac{(p^0 - p^z\,\gamma)^2}{M_N^2} \times \left(\frac{p^z\, Q^2}{(p^0 - p^z\,\gamma) q^0 q^z} + 1 \right)^2 \right] \left(\frac{M_N}{p^0 - p^z\,\gamma} \right) F_{2\tau}^{\rm WI}(x_N, Q^2), \quad (16.48)$$

where $\gamma = \frac{q^z}{q^0} = \sqrt{1 + \frac{4M^2x^2}{Q^2}}$. The choice of xx components of the nucleonic (Eq. (13.62)) and nuclear (Eq. (16.13)) hadronic tensors lead to the expression of $F_{1A,N}^{\rm WI}(x, Q^2)$ as:

$$F_{1A,N}^{\rm WI}(x_A, Q^2) = 2 \sum_{\tau=p,n} AM_N \int d^3r \int \frac{d^3p}{(2\pi)^3} \frac{M_N}{E_N(\vec{p})} \int_{-\infty}^{\mu_\tau} dp^0\, S_h^\tau(p^0, \vec{p}, \rho^\tau(r)) \times \left[\frac{F_{1\tau}^{\rm WI}(x_N, Q^2)}{M_N} + \left(\frac{p^x}{M_N} \right)^2 \frac{F_{2\tau}^{\rm WI}(x_N, Q^2)}{\nu} \right] \quad (16.49)$$

https://doi.org/10.1017/9781108489065.017 Published online by Cambridge University Press

in the case of the nonisoscalar nuclear target. For the electromagnetic interaction channel, the expression of nuclear structure functions are obtained by replacing $F_{i\tau}^{\rm WI}(x_N, Q^2);\ (i = 1,2)$ functions with $F_{i\tau}^{\rm EM}(x_N, Q^2);\ (i = 1,2)$.

Now by using the xy components of the nucleonic (Eq. (13.62)) and nuclear (Eq. (16.13)) hadronic tensors in Eq. (16.44), the parity violating nuclear structure function is obtained as:

$$\begin{aligned} F_{3A,N}^{\rm WI}(x_A, Q^2) &= 2A \sum_{\tau=p,n} \int d^3r \int \frac{d^3p}{(2\pi)^3} \frac{M_N}{E_N(\vec{p})} \int_{-\infty}^{\mu_\tau} dp^0 S_h^\tau(p^0, \vec{p}, \rho^\tau(r)) \\ &\times \frac{q^0}{q^z} \left(\frac{p^0 q^z - p^z q^0}{p \cdot q} \right) F_{3\tau}^{\rm WI}(x_N, Q^2), \end{aligned} \tag{16.50}$$

for a nonisoscalar nuclear target.

For an isoscalar target, the factor of 2 in Eqs. (16.48), (16.49), and (16.50), will be replaced by 4 and the contribution will come from the nucleon's hole spectral function $S_h(p^0, \vec{p}, \rho(r))$ instead of the individual contribution from proton and neutron targets in $S_h^\tau(p^0, \vec{p}, \rho^\tau(r));\ (\tau = p, n)$.

Furthermore, the intermediate vector bosons may interact with virtual mesons like π and ρ, being exchanged between nucleons. Therefore, the mesonic effect have also been incorporated in the Aligarh–Valencia model and are discussed in the following sub-subsection.

Mesonic cloud contribution

There are virtual mesons (mainly pion and rho mesons) associated with each nucleon bound inside the nucleus. This mesonic cloud gets strengthened by the strong attractive nature of the nucleon–nucleon interaction, which leads to a reasonably good probability of interaction of virtual bosons (IVB) with a meson instead of a nucleon [809, 799]. Although the contribution from the pion cloud is larger than the contribution from the rho meson cloud, the rho contribution is non-negligible, and both of them are positive in the entire region of x. The mesonic contribution is smaller in lighter nuclei, while it becomes more pronounced in heavier nuclear targets. The effect of including the spectral function leads to a reduction in the nuclear structure function from the free nucleon structure function, while the inclusion of the mesonic cloud contribution leads to an enhancement of the nuclear structure function, and can explain the experimental data [809, 851, 869].

To obtain the contribution from the virtual mesons, the neutrino self-energy is evaluated by considering a diagram similar to the one shown in Figure 16.10 using a meson propagator instead of a nucleon propagator. These mesons arise in the nuclear medium through particle–hole, delta–hole $(1\Delta - 1h)$, $1p1h - 1\Delta 1h$, etc. interactions as depicted in Figure 16.14.

In the case of mesons, we replace

$$-2\pi \frac{M}{E_N(\vec{p})} S_h(p_0, \vec{p}, \rho(r))\ W_N^{\mu\nu}(p, q)$$

in Eq. (16.44) by

$$\mathrm{Im} D_i(p)\ \theta(p_0)\ 2W_i^{\mu\nu}(p, q)$$

https://doi.org/10.1017/9781108489065.017 Published online by Cambridge University Press

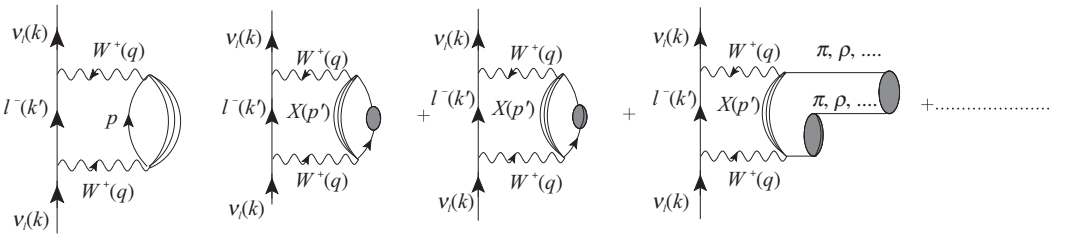

Figure 16.14 Neutrino self-energy diagram accounting for neutrino–meson DIS (a) the bound nucleon propagator is substituted with a meson (π or ρ) propagator (b) by including particle–hole $(1p\text{–}1h)$, delta–hole $(1\Delta\text{–}1h)$, $1p1h - 1\Delta1h$, etc. interactions.

that leads to the following expression:

$$W^{\mu\nu}_{A,i} = 3\int d^3r \int \frac{d^4p}{(2\pi)^4}\,\theta(p_0)(-2)\,\mathrm{Im}D_i(p)\,2m_i W^{\mu\nu}_i(p,q), \tag{16.51}$$

where $i = \pi, \rho$, is a factor of 3 because of the three charge states of mesons. $D_i(p)$ is the meson propagator in the nuclear medium which is given by:

$$D_i(p) = [{p_0}^2 - \vec{p}^{\,2} - m_i^2 - \Pi_i(p_0, \vec{p})]^{-1}, \tag{16.52}$$

with the mass of meson m_i and meson self-energy

$$\Pi_\pi(p_0,\vec{p}) = \left(\frac{f^2}{m_\pi^2}\right)\frac{F_\pi^2(p)\vec{p}^{\,2}\Pi^*_\pi(p)}{1-\left(\frac{f^2}{m_\pi^2}\right)V'_L(p)\Pi^*(p)},\ \Pi_\rho(p^0,\vec{p}) = \left(\frac{f^2}{m_\pi^2}\right)\frac{C_\rho\ \vec{p}^{\,2}\Pi^*_\rho(p)\ F_\rho^2(p)}{1-\frac{f^2}{m_\pi^2}V'_T(p)\Pi^*(p)}. \tag{16.53}$$

Coupling constant $f = 1.01$, $C_\rho = 3.94$; $V'_L(p)$ ($V'_T(p)$) is the longitudinal (transverse) part of the spin–isospin interaction which is responsible for the enhancement in the meson structure function and $\Pi^*_i(p)$ is the irreducible meson self-energy that contains the contribution of particle–hole and delta–hole excitations. $F_i(p)$ is the $\pi NN/\rho NN$ form factor which is given by:

$$F_i(p) = \frac{(\Lambda_i^2 - m_i^2)}{(\Lambda_i^2 + \vec{p}^{\,2})} \tag{16.54}$$

with the parameter $\Lambda_i = 1$ GeV. It must be pointed out that the value of parameters Λ_π and Λ_ρ which is used in the expressions of πNN and ρNN form factors given in Eq. (16.53), respectively, is taken to be 1 GeV. This choice has been made in order to explain the experimental data from JLab [788] and other experiments performed using the charged lepton beam induced DIS processes on several nuclear targets. A detailed discussion is given in Refs.[851, 869, 822].

https://doi.org/10.1017/9781108489065.017 Published online by Cambridge University Press

Equation (16.51) also contains the contribution of the mesonic contents of the nucleon. Since these mesonic contents are already contained in the sea contribution of nucleons, the mesonic contribution of the nucleon is to be subtracted from Eq. (16.51) in order to calculate the contribution from the meson excess in the nuclear medium. This is obtained by replacing $\mathrm{Im}D_i(p)$ by $\delta\mathrm{Im}D_i(p)$ [809] as

$$\mathrm{Im}D_i(p) \;\rightarrow\; \delta\mathrm{Im}D_i(p) \equiv \mathrm{Im}D_i(p) - \rho \;\left.\frac{\partial \mathrm{Im}D_i(p)}{\partial\rho}\right|_{\rho=0}. \tag{16.55}$$

Therefore, the actual mesonic contribution is given by

$$W^{\mu\nu}_{A,i} = 3\int d^3r \int \frac{d^4p}{(2\pi)^4}\,\theta(p_0)(-2)\,\delta\mathrm{Im}D_i(p)\,2m_i W^{\mu\nu}_i(p,q)\,. \tag{16.56}$$

Following the same procedure as in the case of nucleon, one may also obtain the expressions of mesonic nuclear structure functions $F^{WI}_{i'A,i}(x,Q^2)(x,Q^2);\ (i'=1,2)$:

$$\begin{aligned} F^{WI}_{2A,i}(x,Q^2) \;=\; & -6\kappa\int d^3r\int\frac{d^4p}{(2\pi)^4}\,\theta(p^0)\,\delta\mathrm{Im}D_i(p)\,2m_i\left(\frac{m_i}{p^0\;-\;p^z\,\gamma}\right)\times \\ & \left[\frac{Q^2}{(q^z)^2}\left(\frac{|\vec{p}|^2\;-\;(p^z)^2}{2m_i^2}\right)+\frac{(p^0\;-\;p^z\,\gamma)^2}{m_i^2}\right. \\ & \left.\times\left(\frac{p^z\,Q^2}{(p^0\;-\;p^z\,\gamma)q^0q^z}\;+\;1\right)^2\right]\;F^{WI}_{2i}(x_i), \end{aligned} \tag{16.57}$$

and

$$\begin{aligned} F^{\mathrm{WI}}_{1A,i}(x,Q^2) \;=\; & -2\kappa AM\int d^3r\int\frac{d^4p}{(2\pi)^4}\theta(p^0)\,\delta\mathrm{Im}D_i(p)\,2m_i\left[\frac{F^{\mathrm{WI}}_{1i}(x_i)}{m_i}\right. \\ & \left.+\;\frac{|\vec{p}|^2\;-\;(p^z)^2}{2(p^0\,q^0\;-\;p^z\,q^z)}\frac{F^{\mathrm{WI}}_{2i}(x_i)}{m_i}\right], \end{aligned} \tag{16.58}$$

where $\kappa = 1$ for pions and $\kappa = 2$ for rho mesons, $x_i = -\frac{Q^2}{2p\cdot q}$ which carries a negative sign because meson's and nucleon's momenta are opposite in direction. Notice that the ρ-meson has an extra factor of 2 compared to pionic contribution because of the two transverse polarizations of the ρ-meson.

For pionic PDFs, different parameterizations are available in literature such as GRV [873], CTEQ5L [874], SMRS [875], Conway [876], MRST98 [877], etc., which are used while performing numerical calculations. The partonic structure of a pion has been experimentally observed in the Drell–Yan scattering process of pions from bound nucleons in experiments, like E615 [876], NA3 [878], NA10 [879], etc. The Drell–Yan mechanism provides information about the pion's partonic structure in the region of valence quarks while in the region corresponding to sea quarks, data are available from the deep inelastic scattering processes [873].

https://doi.org/10.1017/9781108489065.017 Published online by Cambridge University Press

16.5.3 Kulagin–Petti model

Kulagin and Petti in a series of papers have developed a model for calculating various nuclear effects in the DIS of charged leptons and (anti)neutrinos from nuclear targets [799, 800, 880, 843]. In this model, the nuclear hadronic tensor $W^A_{\mu\nu}$ is written as:

$$W^A_{\mu\nu}(P_A,q) = \sum_{\tau=p,n}\int \frac{d^4p}{(2\pi)^4}\ \mathrm{Tr}\left[\widehat{\mathcal{W}}^N_{\mu\nu}(p,q)\mathcal{A}^N(p;A)\right], \tag{16.59}$$

where $W^A_{\mu\nu}(P_A,q)$ is the nuclear tensor for nucleus A with momentum P_A and $\widehat{\mathcal{W}}^N_{\mu\nu}(p,q)$ is the nucleon tensor for a bound nucleon. $\mathcal{A}^N(p;A)$ is the probability distribution for finding the nucleon with momentum p in the nucleus A given by:

$$\mathcal{A}^N_{\alpha\beta}(p;A) = \int \mathrm{d}t\,\mathrm{d}^3\vec{r}e^{ip_0t-i\vec{p}\cdot\vec{r}}\langle A|\overline{\Psi}^N_\beta(t,\vec{r})\,\Psi^N_\alpha(0)|A\rangle. \tag{16.60}$$

Assuming the nucleons to be nonrelativistic, Eq. (16.59) is simplified to be [799]

$$\frac{W^A_{\mu\nu}(P_A,q)}{A} = \sum_{\tau=p,n}\int \frac{d^4p}{(2\pi)^4}\frac{M}{M+E}\mathcal{P}^\tau(E,\vec{p})\,W^\tau_{\mu\nu}(p,q), \tag{16.61}$$

where $W^A_{\mu\nu}$ and $W^N_{\mu\nu}$ are given in Eqs. (16.59), (16.61), and (13.62). $\mathcal{P}^\tau(E,\vec{p}),\ (\tau=p,n)$ is the spectral function of the nucleon determined from the $(e,e'N)$ reaction and is given by

$$\mathcal{P}(E,\vec{p}) = 2\pi\sum_n |\langle (A-1)_n,-\vec{p}\,|\psi(\vec{p})|\,A\rangle|^2\,\delta\left(E+E_n^{A-1}+E_R-E_0^A\right), \tag{16.62}$$

where $E_R = \frac{p^2}{2M_{(A-1)}}$ is the recoil energy of the residual nucleus and E is the energy of the nucleon in the $(e,e'N)$ reaction. E_n^{A-1} is the energy of the residual nucleus and E_0^A is the ground state energy of the target nucleus. $\mathcal{P}(E,\vec{p})$ is calculated using the ground state and its excitations using a mean field as well as the two nucleon short range correlations (SRC). The spectral function $\mathcal{P}(E,\vec{p})$ is expressed as:

$$\mathcal{P}_0(E,\vec{p}) = \mathcal{P}_{\mathrm{MF}}(E,\vec{p}) + \mathcal{P}_{\mathrm{cor}}(E,\vec{p}). \tag{16.63}$$

with

$$\mathcal{P}_{\mathrm{MF}}(E,\vec{p}) = 2\pi\, n_{\mathrm{MF}}(\vec{p})\delta\left(E+E^{(1)}+E_R(\vec{p})\right), \tag{16.64}$$

https://doi.org/10.1017/9781108489065.017 Published online by Cambridge University Press

corresponding to the mean field (MF). $\mathcal{P}_{\rm cor}(E,\vec{p})$ is the contribution from nucleon–nucleon short range correlations and described by the authors of Ref. [881]. The normalization of $\mathcal{P}(E,\vec{p})$ is given by:

$$\int \frac{d^4p}{(2\pi)^4}\mathcal{P}^{p,n}(E,\vec{p}) = (Z,N). \tag{16.65}$$

Using the expressions discussed in this section, the following results are obtained [799]:

$$F_T^A(x,Q^2) = \sum_{\tau=p,n}\int \frac{d^4p}{(2\pi)^4}\mathcal{P}^{\tau}(E,\vec{p})\,\left(1+\frac{\gamma p_z}{M}\right)\left(F_T^{\tau}+\frac{2x'^2\vec{p}_{\perp}^{\,2}}{Q^2}F_2^{\tau}\right), \tag{16.66a}$$

$$F_L^A(x,Q^2) = \sum_{\tau=p,n}\int \frac{d^4p}{(2\pi)^4}\mathcal{P}^{\tau}(E,\vec{p})\,\left(1+\frac{\gamma p_z}{M}\right)\left(F_L^{\tau}+\frac{4x'^2\vec{p}_{\perp}^{\,2}}{Q^2}F_2^{\tau}\right), \tag{16.66b}$$

$$\gamma^2F_2^A(x,Q^2) = \sum_{\tau=p,n}\int \frac{d^4p}{(2\pi)^4}\mathcal{P}^{\tau}(E,\vec{p})\,\left(1+\frac{\gamma p_z}{M}\right)\left(\gamma'^2+\frac{6x'^2\vec{p}_{\perp}^{\,2}}{Q^2}\right)F_2^{\tau}. \tag{16.67}$$

$$xF_3^A(x,Q^2) = \sum_{\tau=p,n}\int \frac{d^4p}{(2\pi)^4}\mathcal{P}^{\tau}(E,\vec{p})\,\left(1+\frac{p_z}{\gamma M}\right)x'F_3^{\tau}, \tag{16.68}$$

where in the integrand, F_i^{τ} $(i = T,L,2,3)$ are the structure functions of the bound proton $(\tau = p)$ and neutron $(\tau = n)$ with the four momentum $p = (M+E,\vec{p})$; $\vec{p}_{\perp}$ is the transverse component of the nucleon momentum. The Bjorken variable for the bound nucleon is given by

$$x' = \frac{x}{[1+\frac{(E+\gamma p_z)}{M}]} \quad \text{with} \quad \gamma' = \sqrt{1+\frac{4x'^2p^2}{Q^2}}.$$

In this model, the pionic contribution to the nuclear hadronic tensor is evaluated and given by:

$$W_{\mu\nu}^{\pi}(P_A,q) = \frac{1}{2}\int \frac{d^4k}{2\pi^4}D_{\pi}(k)W_{\mu\nu}^{\pi}(k,q), \tag{16.69}$$

where $W_{\mu\nu}^{\pi}(k,q)$ is the hadronic tensor of the pion with momentum k. $D_{\pi}(k)$ describes the momentum distribution of pions in a nucleus [799].

Shadowing effect

The nuclear shadowing/antishadowing is generally understood as arising due to the coherent scattering of hadrons produced in the hadronization process of mediating vector bosons. The destructive interference of the amplitudes due to the multiple partons scattering gives shadowing and their constructive interference gives antishadowing. These coherent effects arise when the coherence length is larger than the average distance between the nucleons bound inside the nucleus and the expected coherence time is $\tau_c \geq 0.2\ fm$. However, the shadowing effect

https://doi.org/10.1017/9781108489065.017 Published online by Cambridge University Press

gets saturated if the coherence length becomes larger than the average nuclear radius, that is, in the region of low x. Due to these effects, the nuclear structure functions are modified in the low region of x [851]. The shadowing effect is different in electromagnetic and weak processes [822]. This is because the electromagnetic and weak interactions take place through the interaction of photons and $W^{\pm}/Z^0$ bosons, respectively, with the target hadrons and the hadronization processes of photons and $W^{\pm}/Z^0$ bosons are different. Moreover, in the case of weak interaction, the additional contribution of the axial current which is not present in the case of electromagnetic interaction may influence the behavior of $F_{2A}^{\rm WI}(x,Q^2)$, especially if pions also play a role in the hadronization process through PCAC. Furthermore, in this region of low x, sea quarks also play an important role which could be different in the case of electromagnetic and weak processes. For example, the sea quark contribution, though very small, is not same for $F_2^{\rm EM}(x,Q^2)$ and $F_2^{\rm WI}(x,Q^2)$ even at the free nucleon level and could evolve differently in a nuclear medium. Generally, the shadowing effect is understood using the Glauber–Gribov multiple scattering theory.

For example, the nuclear structure function incorporating the shadowing effect $F_{iA,shd}^{EM/WI}(x,Q^2)$ may be defined as

$$F_{iA,shd}^{EM/WI}(x,Q^2) = \delta R_i(x,Q^2) \times F_{i,N}^{EM/WI}(x,Q^2), \tag{16.70}$$

where $i = 1,2,3$ and $\delta R_i(x,Q^2)$ is the shadowing correction factor discussed in Ref. [799]. The details are beyond the scope of this book.

16.5.4 Isoscalarity corrections: Phenomenological approach

In the case of heavier nuclear targets, where neutron number ($N = A - Z$) is larger than the proton number (Z) and their densities are also different, isoscalarity corrections become important. As most of the $\nu_l/\bar{\nu}_l$ experiments use heavy nuclear targets ($N \neq Z$), phenomenologically, the isoscalarity correction is taken into account by multiplying the experimental results with a correction factor defined as

$$R_A^{\rm Iso}(x) \quad = \quad \frac{0.5A(1+y(x))}{N(Z/N+y(x))}, \tag{16.71}$$

where $y(x)$ is the ratio of (free) neutron to proton cross sections at a particular value of x. As an example at $x = 0.25$ with the ratio of neutrino cross sections off neutron and protons $y(x) = \frac{\sigma^{\nu n}}{\sigma^{\nu p}} = 1.7$, $R_A^{\rm Iso}(x)$ would be 0.98 for Fe and 0.948 for Pb. Although the non-isoscalarity of a nucleus is considered by some to be a 'nuclear effect', this neutron excess can simply hide the more subtle nuclear effects, and therefore should be properly accounted for.

There are also other phenomenological methods to take into account the isoscalarity correction, for example by taking into account the experimental results for a nonisoscalar nuclear target with a correction factor defined as

$$R_A^{\rm Iso} \quad = \quad \frac{[F_2^{\nu/\bar{\nu}p} + F_2^{\nu/\bar{\nu}n}]/2}{[ZF_2^{\nu/\bar{\nu}p} + (A-Z)F_2^{\nu/\bar{\nu}n}]/A}, \tag{16.72}$$

https://doi.org/10.1017/9781108489065.017 Published online by Cambridge University Press

where Z is the atomic number of the target nucleus, $F_2^{\nu/\bar{\nu}p}$ and $F_2^{\nu/\bar{\nu}n}$ are the weak structure functions for the proton and the neutron, respectively.

The per nucleon nuclear structure function is then compared with the structure function for the isoscalar nucleon target which is obtained from the proton data or deuteron data after applying deuteron correction.

16.6 Results and Discussions

In this section, a few results on nuclear structure functions obtained by using the model of Aligarh–Valencia group (discussed in Subsections 16.5.1, 16.5.2, and 16.5.3) are presented. This model describes the nuclear structure functions $F_{iA}^{EM/WI}(x_A, Q^2)$ $(i = 1-3)$ in terms of the nucleon structure functions $F_{iN}^{EM/WI}(x_N, Q^2)$ convoluted with the spectral function which takes into account Fermi motion, binding energy, and nucleon correlation effects followed by the mesonic and shadowing effects. For the evaluation of $F_{iN}^{EM/WI}(x_N, Q^2)$ at the leading order (LO), free nucleon PDFs are used. The results presented here are obtained with the nucleonic PDF parameterizations of MMHT [552] as well as CTEQ6.6 in the MS-bar scheme [551]. $F_{iA,\pi}^{EM/WI}(x, Q^2)$ and $F_{iA,\rho}^{EM/WI}(x, Q^2)$ are the structure functions having pion and rho mesons contributions. In the literature, various pionic PDFs parameterizations are available like that of Gluck et al. [873], Wijesooriya et al. [874], Sutton et al. [875], Conway et al. [876], etc. The numerical results presented here are with the pionic PDF parameterization of Gluck et al. [873]. To evaluate the nucleon structure functions in the kinematic region of low and moderate Q^2, where the higher order perturbative corrections and the non-perturbative effects become important, PDF evolution is performed up to NNLO and the target mass correction effect is incorporated in the calculations. For the evolution of nucleon PDFs at the next-to-leading order (NLO) and next-to-next-to-leading order (NNLO) obtained from the leading order, the works of Vermaseren et al. [581] and Moch et al. [589, 588] have been followed. The target mass correction effect has been included following the method of Schienbein et al. [591]. The theoretical results are compared with the available experimental data. The total nuclear structure functions including all contributions is defined as:

$$F_{iA}^{EM/WI}(x, Q^2) = \underbrace{F_{iA,N}^{EM/WI}(x, Q^2)}_{\text{spectral function}} + \underbrace{F_{iA,\pi}^{EM/WI}(x, Q^2) + F_{iA,\rho}^{EM/WI}(x, Q^2)}_{\text{mesonic contributions}} + \underbrace{F_{iA,shd}^{EM/WI}(x, Q^2)}_{\text{shadowing effect}} \quad (16.73)$$

for $i = 1-2$. In this model, the full expression for the parity violating weak nuclear structure function is given by,

$$F_{3A}^{\text{WI}}(x, Q^2) = \underbrace{F_{3A,N}^{\text{WI}}(x, Q^2)}_{\text{spectral function}} + \underbrace{F_{3A,shd}^{\text{WI}}(x, Q^2)}_{\text{shadowing effect}}. \quad (16.74)$$

Notice that this structure function has no mesonic contribution and the contribution to the nucleon structure function comes from the valence quarks distributions.

In Figure 16.15, the results for the ratio $R(x, Q^2) = \frac{F_{iA}^{\text{WI}}(x,Q^2)}{F_{iN}^{\text{WI}}(x,Q^2)}$; $(i = 2, 3)$ of nuclear structure functions to the free nucleon structure functions are presented at different values of x in iron and lead which are treated as isoscalar. Numerical calculations have been performed at NNLO by using the MMHT nucleon PDF parameterization [552]. In the figure, theoretical

https://doi.org/10.1017/9781108489065.017 Published online by Cambridge University Press

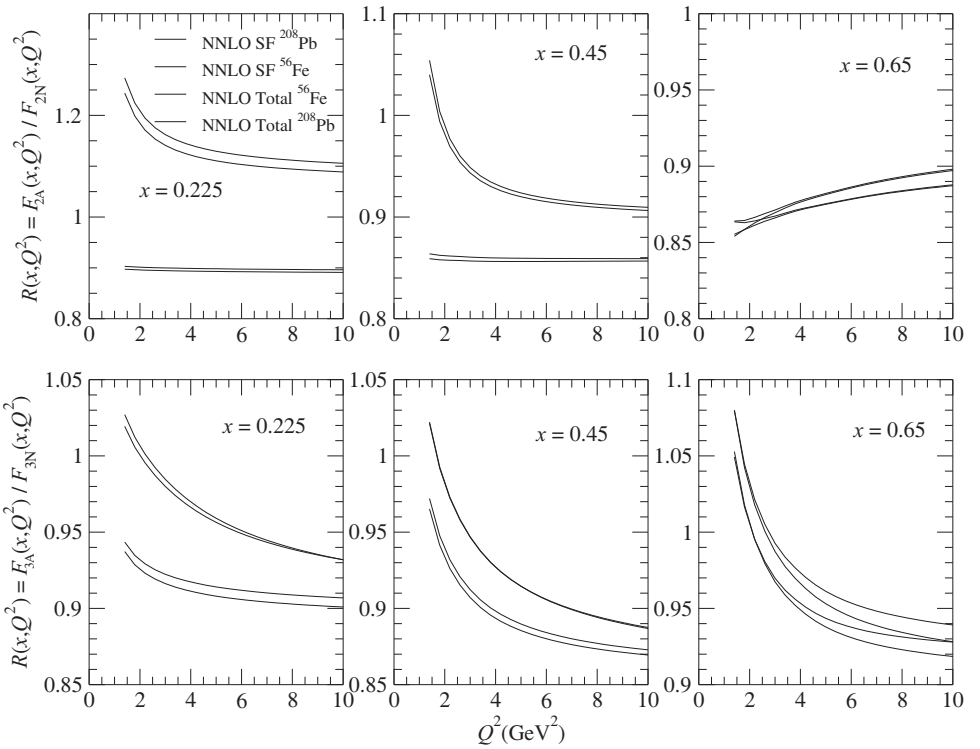

Figure 16.15 $R(x,Q^2) = \frac{F_{iA}^{\rm WI}(x,Q^2)}{F_{iN}^{\rm WI}(x,Q^2)}$; $(i = 2,3)$ vs. Q^2 in ^{56}Fe and ^{208}Pb using the full model. The results are obtained by using MMHT nucleon PDFs parameterization [552] at NNLO (solid line) following the works of Vermaseren et al. [581] and Moch et al. [589, 588] for the free nucleon target; for the nuclear targets, the results are obtained with only the spectral function and the full model.

results are presented by taking into account nuclear effects like Fermi motion, binding energy, and nucleon correlations through spectral function ('NNLO SF') as well as for the full calculations ('NNLO total') which incorporate the mesonic contributions and shadowing effect. One may notice that the ratio $R(x,Q^2)$ is not unity in the entire range of x and Q^2 showing the modification of nuclear structure functions in the nuclear medium. The contributions of mesons is found to be important in the region of low and intermediate x and decreases with the increase in x. Moreover, it is important to point out that as there is no mesonic contribution in $F_{3A}^{\rm WI}(x,Q^2)$, the difference in the results of the spectral function only and the full model (which has contribution from the shadowing effect only) is comparatively smaller than $F_{2A}^{\rm WI}(x,Q^2)$. It is also noticeable that the nuclear medium effects on $R(x,Q^2)$ are larger in lead due to the mass dependence of nuclear medium effects.

In Figure 16.16, the results are presented for $F_{2A}^{\rm WI}(x,Q^2)$ vs. x in ^{12}C, ^{56}Fe, and ^{208}Pb, for isoscalar nuclear targets at different values of Q^2. The results are obtained using the spectral function (dashed line), mesonic effect (dash-dotted line), and the final result by including the shadowing and antishadowing effects as shown by the solid line. The mesonic contributions give an enhancement in the nuclear structure functions which is significant in the low and

https://doi.org/10.1017/9781108489065.017 Published online by Cambridge University Press

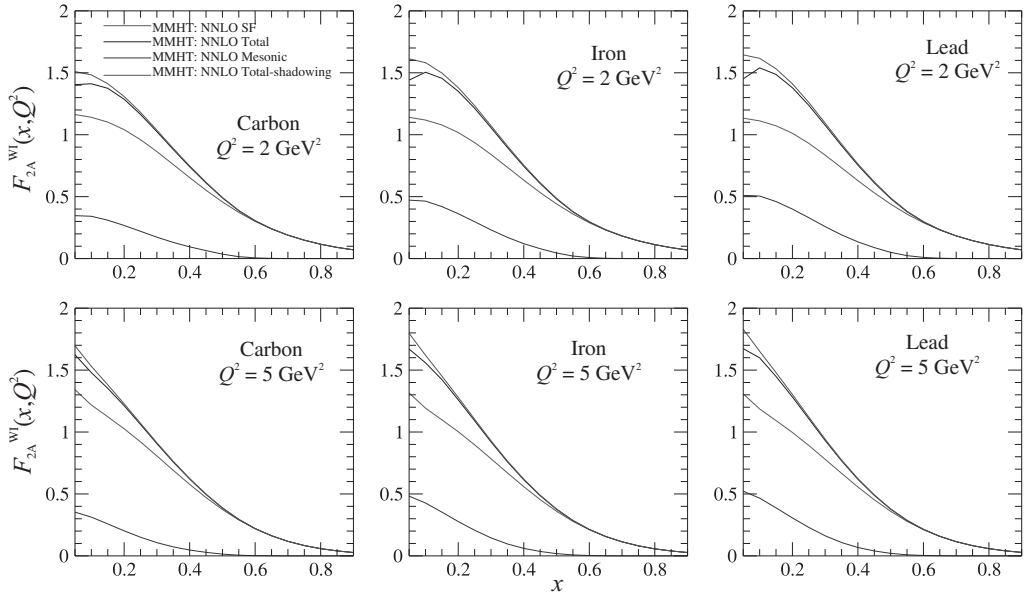

Figure 16.16 Results are shown for the weak nuclear structure function $F_{2A}^{\rm WI}(x, Q^2)$ vs. x at $Q^2 = 2,\ 5\ {\rm GeV}^2$, in ^{12}C, ^{56}Fe and ^{208}Pb for **(i)** only the spectral function (dashed line), **(ii)** only the mesonic contribution (dash-dotted line) using Eq. (16.57), **(iii)** the full calculation (solid line) using Eq. (16.73) as well as **(iv)** the double-dash-dotted line is the result without shadowing and antishadowing effects. The numerical calculations has been performed at NNLO by using the MMHT [552] nucleon PDFs parameterizations.

intermediate region of x. Moreover, the effect is more pronounced at low Q^2 and becomes larger with increase in mass number A. To depict the coherent nuclear effects (shadowing and antishadowing effects) which cause a suppression in the structure functions at low x, the results are shown with the double-dash-dotted line, and it may be observed that with the increase in mass number of the nuclear target (^{56}Fe vs. ^{208}Pb), the strength of suppression becomes larger. For the (anti)neutrino scattering cross sections and structure functions, high statistics measurements have been done by CCFR [562], CDHSW [561], and NuTeV [566] experiments in iron and by CHORUS [882] collaboration in lead nuclear targets. These experiments have been performed in a wide energy range, that is, $20 \leq E_\nu \leq 350$ GeV and the differential scattering cross sections have been measured. The results for $F_{2A}^{\nu+\bar\nu}(x, Q^2)$ and $xF_{3A}^{\nu+\bar\nu}(x, Q^2)$ are presented in Figures 16.17 and 16.18 treating these nuclei as isoscalar targets. The experimental results are compared with the theoretical results calculated using the full model at NNLO.

https://doi.org/10.1017/9781108489065.017 Published online by Cambridge University Press

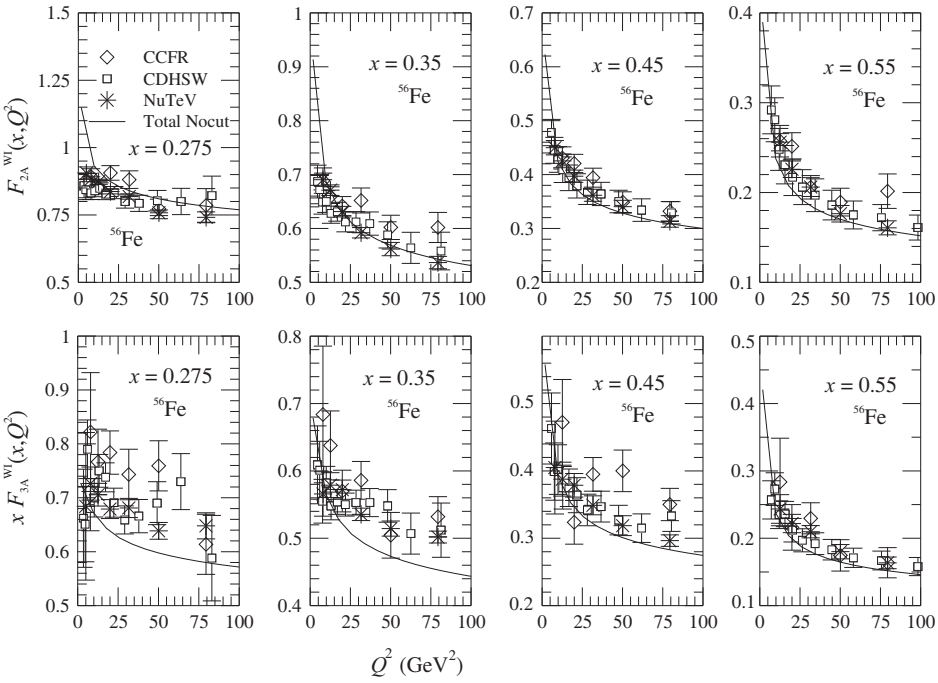

Figure 16.17 $F_{2A}^{\mathrm{WI}}(x, Q^2)$ vs. Q^2 in ^{56}Fe using the full model. The results are obtained by using CTEQ6.6 nucleon PDFs at NLO in the MS-bar scheme (dotted line), MMHT at NLO (dashed line) and NNLO (solid line). The experimental points are the data from CDHSW [561], CCFR [562], and NuTeV [566] experiments.

The agreement among the two results is satisfactory except at very low x and Q^2. We have found that the theoretical results differ from the experimental data in the region of low x and low Q^2; however, with the increase in x and Q^2, they are found to be in reasonably good agreement with the experimental determination.

In Figure 16.19, the variation of nuclear medium effects in the electromagnetic and weak interactions has been shown by using different nuclear targets. The ratio R' deviates from unity in the region of low x even for the free nucleon case which implies the nonzero contribution from strange and charm quarks distributions. However, for $x \geq 0.4$, where the contribution of strange and charm quarks are almost negligible, the ratio approaches unity. Furthermore, if one assumes $s = \bar{s}$ and $c = \bar{c}$, then in the region of small x, this ratio would be unity for an isoscalar nucleon target following the $\left(\frac{5}{18}\right)^{\text{th}}$-sum rule. For heavier nuclear targets like ^{56}Fe and ^{208}Pb, the nuclear medium effects become more pronounced. This shows that the difference in charm and strange quark distributions could be significant in heavy nuclei.

https://doi.org/10.1017/9781108489065.017 Published online by Cambridge University Press

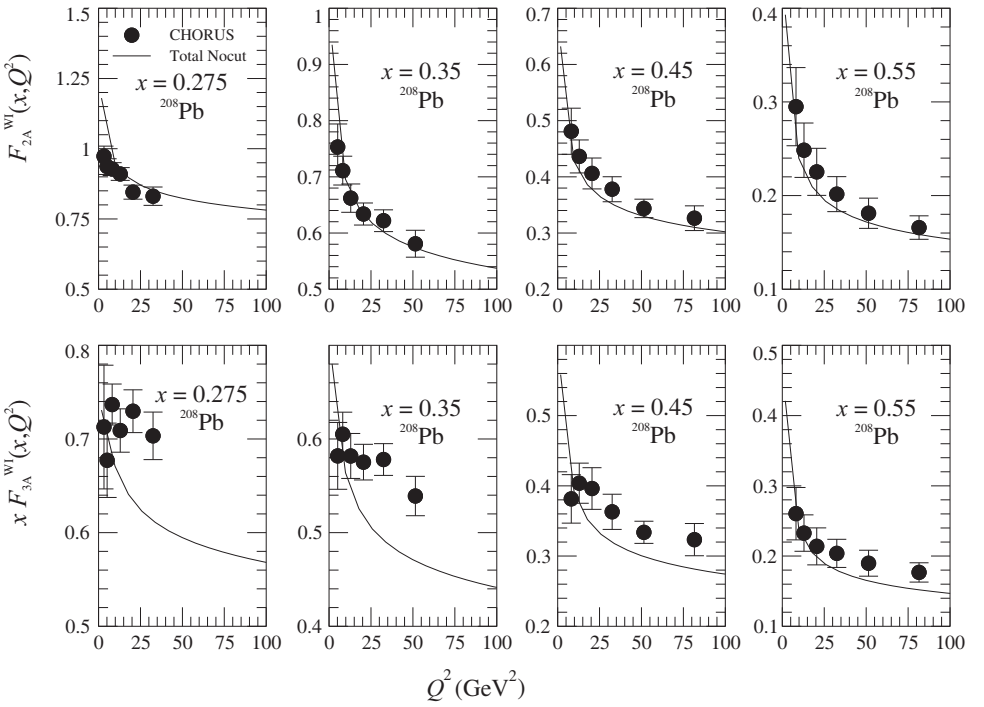

Figure 16.18 $F_{2A}^{\mathrm{WI}}(x, Q^2)$ vs. Q^2 in ^{208}Pb using the full model. The results are obtained using CTEQ6.6 nucleon PDFs at NLO in the MS-bar scheme (dotted line), MMHT at NLO (dashed line) and NNLO (solid line). The experimental points are the data from CHORUS [562].

In Figure 16.20, the results are shown for $\frac{1}{E_\nu}\frac{d^2\sigma_A^{\mathrm{WI}}}{dxdy}$ vs. y for $\nu_l - A$, $(A = ^{56}\mathrm{Fe}, ^{208}\mathrm{Pb})$ scattering at NNLO at different values of x for the incoming beam energy of 35 GeV. Theoretical results are presented for the spectral function only (dashed line), using the full model (solid line) and are compared with the experimental data of NuTeV [566] (top panel) and CHORUS [882] (bottom panel) collaborations. It may be noticed that the mesonic effects are important only in the low and intermediate region of x i.e. $x < 0.65$.

https://doi.org/10.1017/9781108489065.017 Published online by Cambridge University Press

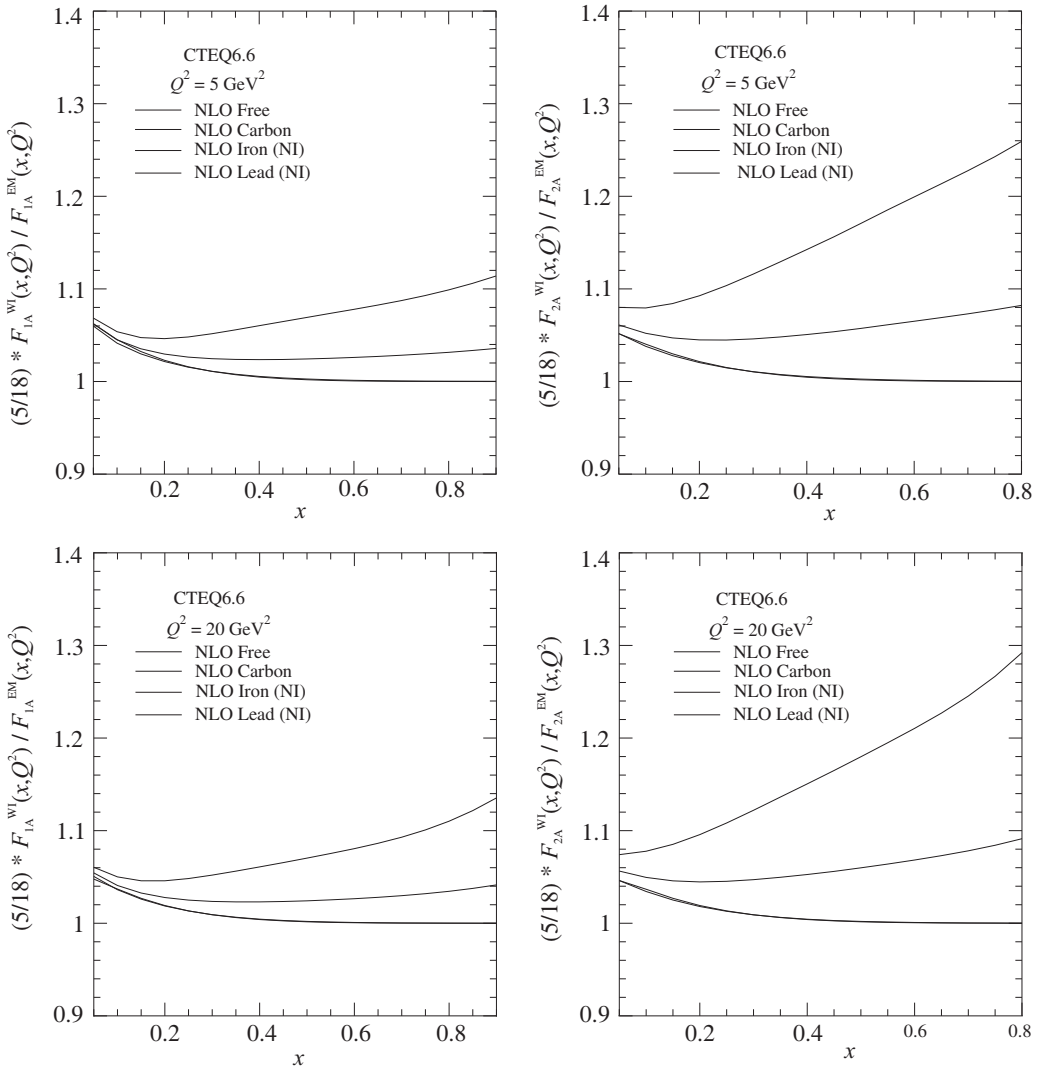

Figure 16.19 Results for the ratio $R'(x,Q^2) = \frac{\frac{5}{18}F_{iA}^{\rm WI}(x,Q^2)}{F_{iA}^{\rm EM}(x,Q^2)}$; $(i = 1,2)$ are obtained by using the full model at NLO in $A = {}^{12}$C, ^{56}Fe and ^{208}Pb at $Q^2 = 5$ and 20 GeV^2. Numerical results are obtained by using the CTEQ6.6 nucleon PDFs in the $\overline{MS}$ scheme [551] (NI stands for nonisoscalar).

Thus, the nuclear medium effects are important in the DIS region and are better phenomenological as well as theoretical models which cover a wide range of x and Q^2 for intermediate and heavy mass nuclei are highly desirable.

https://doi.org/10.1017/9781108489065.017 Published online by Cambridge University Press

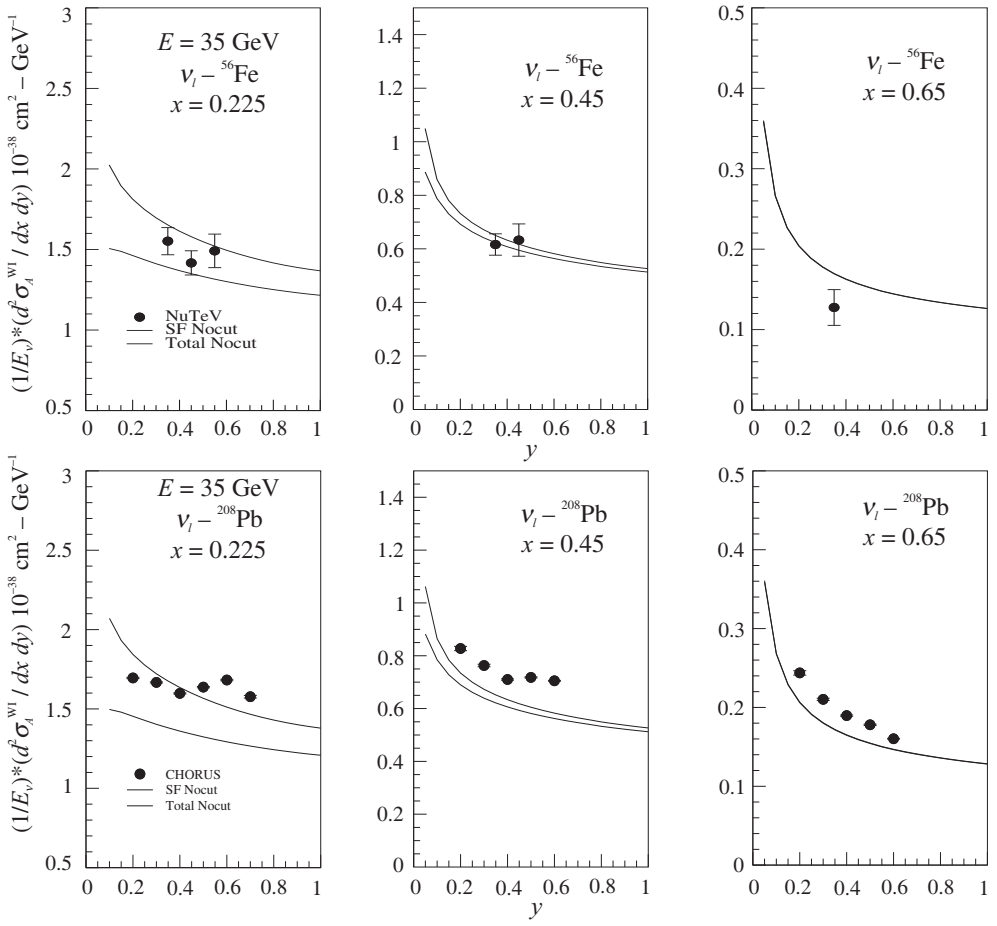

Figure 16.20 $\frac{1}{E_\nu}\frac{d^2\sigma_A^{WI}}{dxdy}$ vs. y are shown at different values of x for the incoming beam of energy $E = 35$ GeV. The numerical results are obtained with the spectral function only (dashed line) and with the full model (solid line) at NNLO, Top panel: for $\nu_l - {}^{56}$Fe and Bottom panel: for $\nu_l - {}^{208}$Pb DIS processes. The results are compared with the experimental data points of NuTeV [566] and CHORUS [882]. Nuclear targets are treated to be isoscalar.

https://doi.org/10.1017/9781108489065.017 Published online by Cambridge University Press